Geophys. J. Int. (1994) **117**, 313–334

The wavelength-smoothing method for approximating broad-band wave propagation through complicated velocity structures

Anthony Lomax*
Seismographic Stations, Department of Geology and Geophysics, University of California at Berkeley, Berkeley, California 94720, USA

Accepted 1993 September 8. Received 1993 July 14; in original form 1993 February 18

SUMMARY

This paper introduces a new, efficient method for approximating broad-band wave propagation in complicated velocity structures. The complete justification and development of this method are not presented, but it is shown that this technique, despite its simplicity, reproduces many expected broad-band, wave-propagation phenomena.

This method, named here the wavelength-smoothing (WS) technique, is based on the computation of wave refraction using Huygens' principle and a frequency-dependent velocity function defined as the wave velocity smoothed over a wavelength across the wavefront. The WS method reduces to geometrical ray theory at high frequency, but also produces broad-band wave phenomena such as dispersion, phase shifting upon reflection and wavelength-dependent scattering. Transmitted refractions, wide-angle reflections and head waves are produced at discontinuities without requiring the matching of boundary conditions. The WS method is subject to some of the limitations of geometrical ray methods including amplitude instability at caustics and incomplete modelling of diffractions near critical regions. Also, wavetype conversions and pre-critical reflections are not produced at internal discontinuities.

The WS technique is an application of physical principles but is intuitively based and not formally derived from basic equations. As a consequence, the completeness and accuracy of the method may be less than that of other techniques. Although a number of tests and comparisons of the method have given satisfactory results, additional investigations to provide further justification and verification are now required.

The WS algorithm requires much less computer time and memory than numerical techniques and may be applied in practice to complicated, 3-D velocity models. A comparison between the WS method and a boundary integral method applied to a 2-D, rough interface model is presented in this paper.

Key words: bodywaves, broad-band waveforms, complex structures, synthetic seismograms, ray tracing.

1 INTRODUCTION

Knowledge of the seismic-velocity structure of the earth's crust and upper mantle, and the description of seismic-wave propagation through these structures, is of fundamental importance for the understanding of many geologic processes. For many years, the modelling of wave propagation in the earth was limited by the state of observation, theory and computational resources to laterally homogeneous structures. Unfortunately, as geologists and seismologists have long recognized, these simple models are inadequate for fully describing realistic crustal and upper mantle structures and for reproducing many observed seismic waveforms. The study of broad-band seismograms in realistic earth models requires methods for modelling broad-band wave propagation from a localized source within an arbitrary, 3-D velocity structure. An optimal method

* Now at: Department of Geophysics, University of Utrecht, P.O. Box 80.021, 3508 TA Utrecht, The Netherlands.

would apply complete waveform physics to complicated velocity models while making efficient use of computational resources.

However, most existing methods for efficiently generating synthetic seismograms produce either approximate, conditional results in complex models or more exact results in highly symmetric models (Aki & Richards 1980). Techniques representative of these two extremes include *ray* methods and *full-waveform* methods such as generalized ray, reflectivity and modal summation. Ray methods produce traveltimes, amplitudes and other features of wavefields in realistic models, but are valid only where the changes in the elastic moduli and density are negligible within one wavelength (Fuchs 1968, Červený, Molotkov & Pšenčík 1977). This restriction limits the ray methods to the study of high-frequency wavefields. Ray methods are also difficult to apply to the analysis of complicated velocity structures since these methods are highly sensitive to small-scale features of the model (Červený 1985a).

Full-waveform methods are efficient and accurate because they make extensive use of analytic solutions to basic equations. Unlike most ray-based techniques, these methods can produce broad-band synthetics; also, they require much less computer time and memory than numerical methods. However, full-waveform methods are valid only for layered models and, with certain extensions, for models with planar, non-parallel interfaces (e.g. Hong & Helmberger 1978; Richards, Witte & Ekstrom 1991) and so cannot be applied to arbitrary velocity structures.

The finite-difference and finite-element methods and other *numerical* techniques (Aki & Richards 1980; Bullen & Bolt 1985) can also in principle model both broad-band wave phenomena and 3-D structures. However, practical, routine application of these methods is limited by computational considerations (Spudich & Archuleta 1987; Frankel 1989). Currently, 3-D applications are restricted to small study volumes relative to wavelength and require the most powerful computers (e.g. Igel *et al.* 1991; Frankel & Vidale 1992).

All of these methods and most other wave-propagation techniques involve derivations from the elasto-dynamic equation of motion or the scalar wave equation. Typically, these derivations are advanced by restricting the model parametrization, by limiting the applicable wave types or wave frequencies, or by neglecting selected terms. The resulting methods are well defined and can be numerically accurate, but are only valid for a limited range of wave phenomena and model geometries.

As an example of the successful application of these methods consider the seismological inference of radial velocity structure within the whole earth (Dziewonski & Anderson 1981; Bullen & Bolt 1985). In this case, full waveform and ray methods developed for a spherical geometry could be used for inversion with good resolution because the 'true' earth structure is apparently close to spherical symmetry and because the typical path lengths of the observed waves are large relative to their wavelengths.

However, few of the presently available methods for approximating wave propagation are valid and practical in complicated, 3-D models representative of the crust and upper mantle of the earth.

To address this shortcoming, an approximate method for modelling of broad-band wave propagation in heterogeneous velocity structures is introduced in this paper. This technique, named the *wavelength-smoothing* (WS) method, has similarities to both ray-tracing and full-waveform techniques. Because the WS method responds directly to velocity variations, it is neither a scalar, nor an elastic formulation, but instead is 'kinematic'. Examples of the application of the WS method have been presented previously (Lomax & Bolt 1992), however, this paper and Lomax (1992) form the first presentation and preliminary validation of the methodology.

2 THE WAVELENGTH-SMOOTHING METHOD

The WS method combines Huygens' principle and wavelength-dependent velocity smoothing to approximate broad-band wave propagation through models with complicated velocity distributions. A broad-band wavefield is constructed by summing the results of independent, time-domain propagation of narrow-band 'wavefields' at many centre frequencies. In the following discussion, terms such as *wave path, wavefront* and *wave location* refer to these narrow-band 'wavefields' and not to the final, broad-band wavefield.

2.1 Basic assumptions and methodology

The WS method is based on two principal assumptions. First, many features of broad-band wave propagation can be modelled by using Huygens' principle to track the motion of *narrow-band wavefronts* at a number of centre frequencies; the narrow-band wavefronts are defined as surfaces of constant phase or traveltime in a narrow-band 'wavefield'. The second assumption is that the velocity of propagation of body waves at a particular frequency and location can be approximated by a *wavelength-averaged velocity,* given by a centrally weighted average of the medium velocity across the narrow-band wavefront, with the width of the weighting function varying in proportion to wavelength (Fig. 1).

Both of these assumptions become strictly valid as infinite frequency is approached because, in this limit, Huygens' principle is equivalent to geometrical ray theory (e.g. Officer 1958) and the wavelength-averaged velocity converges to the local medium velocity. However, the validity of either assumption at finite frequency does not follow immediately from wave physics. In this work these assumptions are justified with theoretical argument and by comparison of results of the WS method with the results of basic wave physics and other wave-propagation techniques.

The motion through time of the narrow-band wavefronts determines *wave paths,* which are similar to the rays of ray theory, but are frequency dependent. The wavelength-dependent smoothing of the medium in the WS algorithm leads to increased stability of wave paths relative to high-frequency ray methods and produces a sensitivity of the waves to larger velocity anomalies within about a wavelength of the wave path (Fig. 2).

After many sets of wave paths at a range of centre

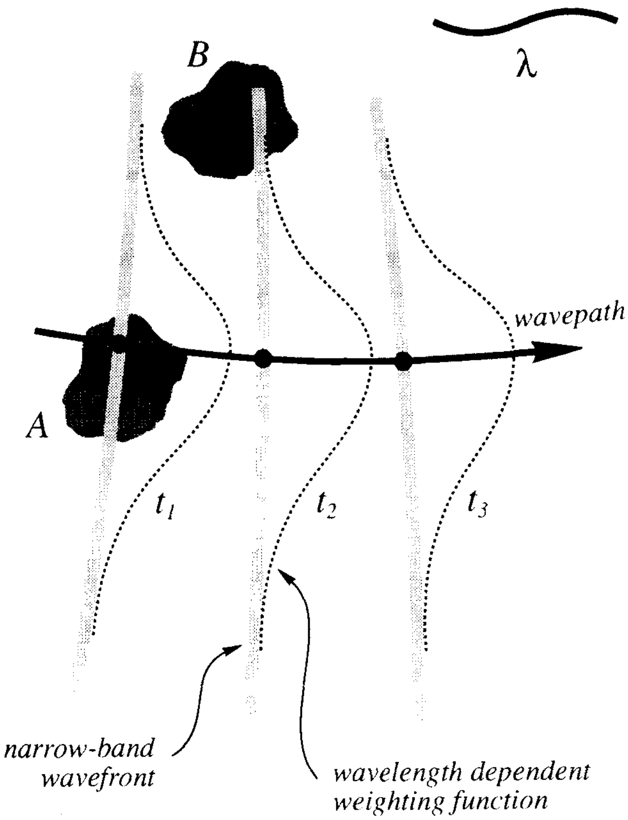

Figure 1. Wave path, wavefront and wavelength-averaged velocity weighting function for three time steps t_1, t_2 and t_3. The perpendicular distance from each point of the wavefront to the corresponding weighting function shows the relative weighting along the wavefront. A centrally peaked weighting function is required so that a region *A* of anomalous velocity close to the wave path has a stronger influence on the change in position and orientation of the wavefront and wave path at each time increment than a region *B* far from the wave path. The approximate wavelength λ is indicated with a sinusoid.

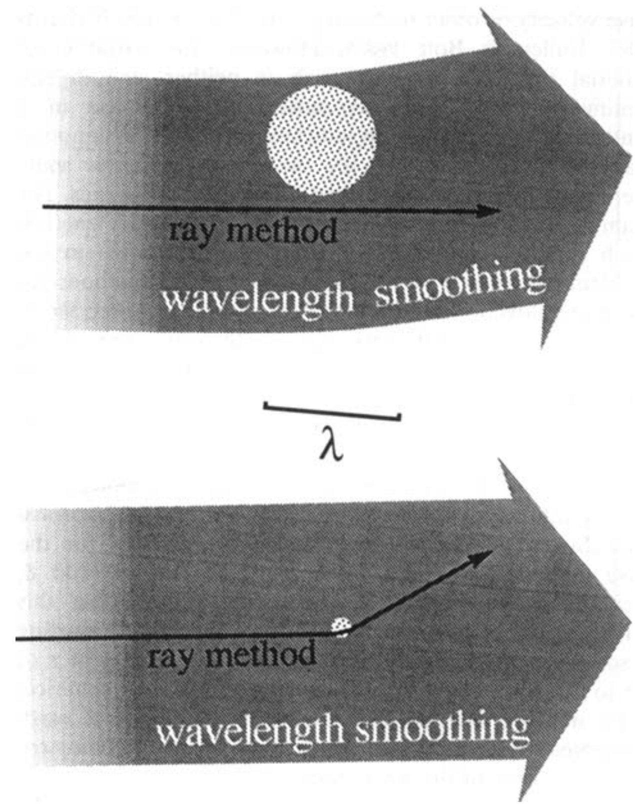

Figure 2. Cartoons showing significant differences between the wavelength smoothing and ray methods. (Top) A ray-theory ray is unperturbed in passing near a velocity anomaly (stippled region), while a WS wave path for wavelength λ will be deflected by the anomaly if the anomalous region is large relative to λ and lies within about a wavelength of the wave path. The wavelength velocity averaging along the wavefront in the WS method causes information from the medium away from the wave path to affect the wave path. (Bottom) A ray-theory ray can be strongly scattered by a small velocity anomaly (stippled region), while a WS wave path for wavelength λ will not be deflected by an anomalous region which is small relative to λ. The wavelength velocity averaging in the WS method smoothes out the effect of small velocity variations.

frequencies have been generated with the WS technique, broad-band waveforms are produced by a summation of the contributions of all wave types at all frequencies arriving at a given receiver location. In a manner similar to the ray method, the traveltime and amplitude of a given wave type are estimated from the traveltime and geometrical spreading of adjacent wave paths of the same wave type passing near the receiver location.

For simplicity, in the current implementation of the WS method, the effective narrow-band wavefront at any time is approximated by an *instantaneous wavefront*, a straight-line segment (2-D) or a plane (3-D) normal to the wave-path direction passing through the *wave-path location*, the position in space of the wave path at any given time. This approximation requires that the radius of curvature of the wavefront is large relative to a wavelength; this is only true in general if the medium is smoothly varying relative to a wavelength. However, with the WS method, the radius of curvature of the narrow-band wavefront will be large *after* the wavelength-averaged velocity smoothing is applied, except in regions within about a wavelength of sources and focusing points.

2.2 Justification of wavelength-averaged velocity

The WS method is based on explicit smoothing of the medium to produce the wavelength-averaged velocity. It is this wavelength-dependent smoothing that makes the WS method a broad-band wave-propagation technique, and distinguishes it from the high-frequency ray methods.

A formal demonstration of the validity of the wavelength-averaged velocity under generally defined conditions for use in a wave-propagation method is not currently available. In the following it is argued that the use of wavelength-dependent velocity smoothing in the present seismological context is justified because this form of smoothing is implicit in the formulation and application of most seismic-wave propagation techniques, and because some effective smoothing of earth properties is predicted by scattering theory.

Most methods for synthesizing seismic-wave propagation require the use of smoothly varying functions to represent wave velocity or other material parameters (Aki & Richards 1980; Bullen & Bolt 1985). However, the variation of material properties in the earth is neither smooth nor continuous: it is rough at most scales; the use of a continuous velocity function indicates an implicit assumption that the propagation of the wavefield performs some averaging or effective smoothing of material properties. For example, ray theory is strictly valid only if the wavelength is much smaller than all other characteristic lengths in the problem (Červený *et al.* 1977). In practice, ray methods are often employed to interpret observations from finite-frequency waves that have passed through complicated velocity structures that are likely to contain features much smaller than the wavelength.

Some form of wavelength-dependent averaging in the earth is also indicated by the analysis of surface waves and normal modes using eigenvibrations. Eigenfrequencies and eigenvibrations can be calculated in a flat layer or spherical earth by integration of the differential equations for the wave motion from some depth d to the surface (Aki & Richards 1980). Bolt & Dorman (1961) show that this numerical integration can be performed accurately starting at some cut-off depth $d = \varepsilon\lambda$. They find that values of ε of 1.5 to 2.1 are adequate for Rayleigh waves in a spherical earth, implying that an integration (or averaging) of earth properties over about one to two wavelengths accounts for the greater part of the wave motion.

An apparent smoothing of material properties by the wavefield is also supported by the results of scattering studies (see Aki & Richards 1980, Chapter 13). The effectiveness of this smoothing is found to be related to the ratio of the characteristic size of elastic inhomogeneities to the wavelength and the ratio of path length to wavelength. When a medium has a characteristic size of inhomogeneity d that is much less than the wavelength λ, it can be replaced with some equivalent, homogeneous medium. When the inhomogeneity size d is much greater than a wavelength λ, the medium is effectively piece wise smooth, and ray methods are applicable. The most difficult case is when inhomogeneity size is comparable to the wavelength $d = O(\lambda)$. In this case diffraction effects are strongest and classical analytic or ray methods may not be valid.

The result of apparent smoothing in the case of small inhomogeneity size leads to the use of wavelength smoothing in the WS method. In an attempt to produce useful, approximate results for all inhomogeneity sizes, including the most difficult case of $d = O(\lambda)$, the smoothing of the velocity structure is explicitly coupled to wavelength. The WS method is applicable to large- or small-inhomogeneity scale relative to the wavelength because in the former case it is the same as ray theory and in the latter it responds to a smooth, averaged velocity structure. Consequently, model roughness is not restricted in the *application* of the WS method and realistic, complicated velocity models can be explored. This is not to say, however, that the *accuracy* of the WS method is independent of model complexity.

2.2.1 *Geometry of wavelength-velocity averaging*

In the WS method the wavelength-dependent velocity for a particular wave path and time is determined by some weighted average across the wavefront of the wave velocity in the medium. The weighting function has a maximum at the wave-path location and decays smoothly to zero far from the wave path (Fig. 1). A weighting function with a maximum at the wave-path location, and a smooth decay to zero away from the wave path, is necessary to suppress the effect of velocity anomalies far from the wave path and is also required to maintain compatibility with ray theory at frequency $f \to \infty$. For simplicity, the width of smoothing is taken independent of distance from the source and receiver.

The wavelength averaging is taken over velocity v instead of another parameter, such as slowness $1/v$, because it is the wave velocity directly that is used to propagate wavefronts in Huygens' principle. Also, in preliminary tests of the WS method at a plane discontinuity, the direct averaging of velocity v resulted in wave paths that more closely matched the predictions of basic wave physics than did, for example, averaging over $1/v$. However, in the WS method Huygens' principle is formally applied only after the wavelength smoothing, and there is some uncertainty as to the optimum form of the smoothing function. Consequently it may be found with further development of the method that a parameter other than v is more appropriate for the smoothing.

The velocity averaging is taken across the wavefront only and not in some volume around the wave-path location, because this is compatible with Huygens' principle, which makes use of material properties only on the wavefront. In addition, the propagation of the waves through time leads to the consideration of material properties in the direction along the wave paths, perpendicular to the surface of the wavefronts.

The consideration of material properties only along the wavefront surface at each time increment is also consistent with the Helmholtz–Kirchhoff integral theorem (Elmore & Heald 1985), which states that the wavefield at an observation point P can be completely determined by an integration of the field over a surface S that surrounds P. In the WS method the instantaneous wavefront at a particular time forms the analogue to the surface S while the wave-path location at a slightly later time is identified with the observation point P; the use of the wavelength-averaged velocity across the wavefront is analogous to the integration of the field on S. Consideration of the Helmholtz–Kirchhoff integral theorem in this context also leads to a weak justification for the general form of the weighting function (Lomax 1992).

2.2.2 *Implementation of wavelength-averaged velocity*

In a 2-D geometry the wavelength-averaged velocity $\bar{v}$ at point $\mathbf{x}_v$ and period T is given by

$$\bar{v}(\mathbf{x}_v, T) = \frac{\int_{-\infty}^{\infty} w(\theta) c[\mathbf{x}(\theta, T)]\, d\theta}{\int_{-\infty}^{\infty} w(\theta)}, \tag{1}$$

where θ is distance along the wavefront away from $\mathbf{x}_v$ expressed in wavelengths, $c(\mathbf{x})$ is the local medium velocity at point $\mathbf{x}$ and $w(\theta)$ is a weighting function. $\mathbf{x}(\theta, T)$ is position along the instantaneous wavefront given by the

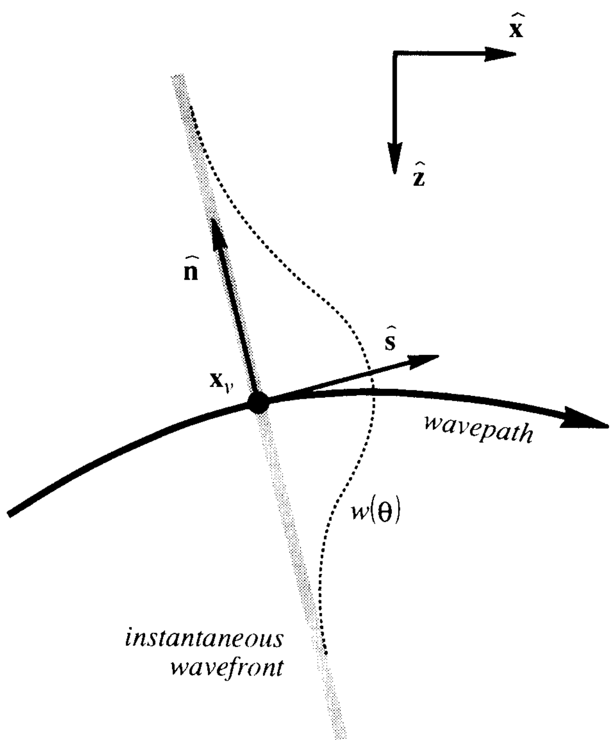

Figure 3. Wavelength-smoothing wave path, instantaneous wavefront, global coordinates $\{x, y\}$, ray location $\mathbf{x}_v$, ray centred coordinates $\{s, n\}$, and schematic weighting function $w(\theta)$.

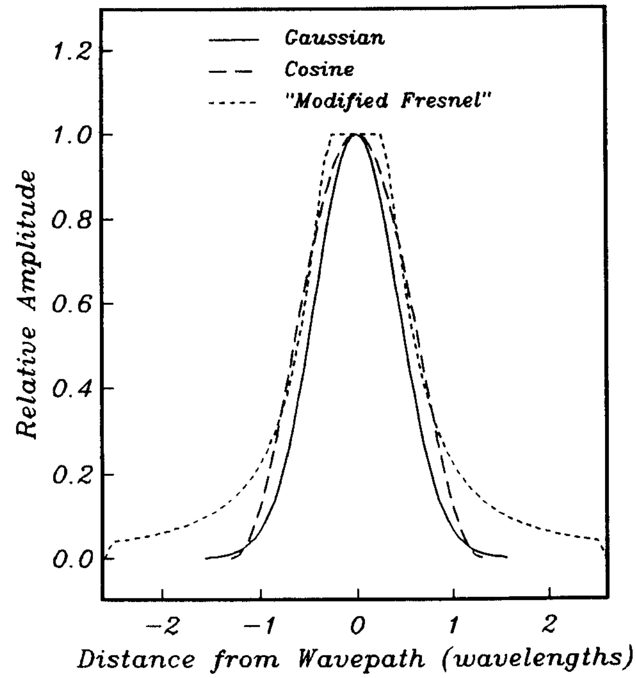

Figure 4. Gaussian ($\alpha = 2.0$) weighting function and cosine and 'modified Fresnel' weighting functions for equivalent α values. The amplitude of the normalized weights are plotted as a function of distance in wavelengths along the instantaneous wavefront away from the wave path.

recursive relation

$$\mathbf{x}(\theta, T) = \mathbf{x}_v + \frac{T}{2\pi}\int_0^{\theta} c[\mathbf{x}(\theta', T)]\, d\theta' \hat{\mathbf{n}}(T), \tag{2}$$

where $\hat{\mathbf{n}}$ is the unit normal at point $\mathbf{x}_v$ to the wave path for period T (Fig. 3). Note from (2) that $d\mathbf{x}/d\theta$ is directly proportional to local medium velocity $c(\mathbf{x})$ and period T. Consequently, the effective width of the velocity smoothing function is a function of the wave period and of the wave velocity *at all points along the instantaneous wavefront*. This means that a region of anomalous velocity near, but not necessarily on the wave path, can affect the width of velocity smoothing, which will affect the future wave-path trajectory.

In the present work only a weighting function $w(\theta)$ with the form of a Gaussian bell is discussed in detail. This Gaussian bell weighting curve is given by

$$w_g(\theta) = \exp[-4\ln 2(\theta/\alpha)^2], \tag{3}$$

where α specifies the half-width of the Gaussian bell in wavelengths. For large $|\theta|$ the Gaussian function $w_g(\theta)$ asymptotically approaches 0.

In Lomax (1992) two additional weighting functions are examined: a cosine bell and a function based on a derivation from the Helmholtz–Kirchhoff integral theorem and referred to as the 'modified Fresnel' function (Fig. 4). The amplitude of all of these functions has a maximum at $\theta = 0$ (location $\mathbf{x}_v$) and decreases away from $\mathbf{x}_v$ in each direction along the wavefront. The Gaussian bell is selected here as a preferred weighting function, but there is some evidence that another functional form may produce better results (Lomax 1992). A more thorough examination of the form of the weighting function is left for future work.

2.2.3 *Discrete representation of equations*

For application on digital computers, the continuous integral along the instantaneous wavefront for the wavelength-averaged velocity (1) is replaced by a sum over a finite set of $2N + 1$ *control points* spaced in proportion to local wavelength along the instantaneous wavefront (Fig. 5):

$$\bar{v}(\mathbf{x}_v, T) = \frac{\sum_{n=-N}^{N} w_n c[\mathbf{x}_n(T)]}{\sum_{n=-N}^{N} w_n}. \tag{4}$$

The location of the control points is given by a discrete version of expression (2):

$$\mathbf{x}_0 = \mathbf{x}_v, \tag{5}$$

$$\mathbf{x}_n = \begin{cases} \mathbf{x}_{n-1} + \dfrac{\theta_{\max} T}{4\pi N} c(\mathbf{x}_{n-1})\hat{\mathbf{n}}; & n = 1, 2, \ldots, N, \\ \mathbf{x}_{n+1} - \dfrac{\theta_{\max} T}{4\pi N} c(\mathbf{x}_{n+1})\hat{\mathbf{n}}; & n = -1, -2, \ldots, -N, \end{cases} \tag{6}$$

where $\theta_{\max}$ is a truncation parameter that specifies the greatest distance in wavelengths along the wavefront at which smoothing is applied. The locations of the control points $\mathbf{x}_n$ are estimated in both directions starting from the location $\mathbf{x}_v$. The distance along the wavefront in wavelengths, θ_n, corresponding to location $\mathbf{x}_n$ is

$$\theta_n = \frac{n\theta_{\max}}{N}, \tag{7}$$

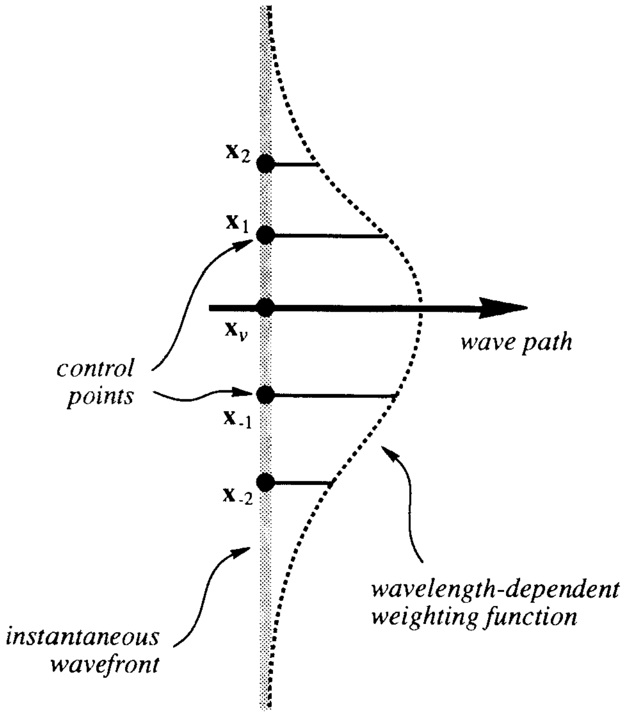

Figure 5. Wavelength-dependent velocity-smoothing calculation for point $\mathbf{x}_v$. Centrally weighted smoothing is applied across an instantaneous wavefront defined by the normal to the wave path.

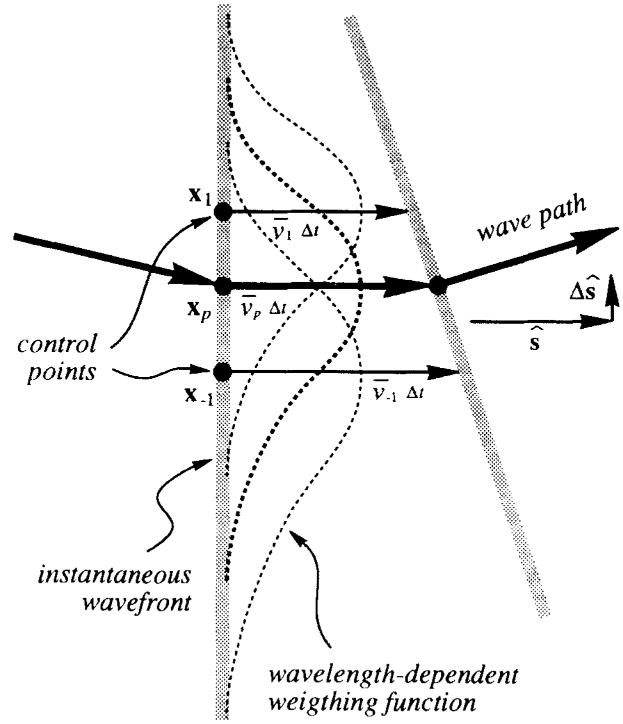

Figure 6. Wavelength-smoothing wave-path-movement calculation. An approximation to Huygens' principle is applied by considering the motion of a point $\mathbf{x}_p$ on the wave path and the two closest control points $\mathbf{x}_{-1}$ and $\mathbf{x}_1$ under the influence of the smoothed velocity $\bar{v}$. This calculation gives the translation $\bar{v}_p\Delta t$ and bending $\Delta\hat{\mathbf{s}}$ of the wave path. At infinite frequency or if no velocity smoothing were applied, this algorithm reduces to the ray method.

and the discrete form of the Gaussian weight function (3) is

$$(w_g)_n = \exp[-4\ln 2(\theta_n/\alpha)^2]. \tag{8}$$

2.3 Movement of wave paths

The change in position of the wavefront location $\mathbf{x}_p$ along the wave path is approximated by

$$\Delta\mathbf{x}_p = \bar{v}_p\,\Delta t\hat{\mathbf{s}}, \tag{9}$$

where $\bar{v}_p$ is the wavelength averaged velocity at $\mathbf{x}_p$, Δt is the time step and $\hat{\mathbf{s}}$ is the unit vector along the propagation direction (Fig. 3).

The change in the direction of $\hat{\mathbf{s}}$ is directly related to the change in direction of the instantaneous wavefront since $\hat{\mathbf{s}}$ is always normal to the front by definition. The change in direction of the front is approximated by the difference in movement between the first control points on each side of the wave location $\mathbf{x}_0 = \mathbf{x}_p$ during one time step (Fig. 6):

$$\Delta\hat{\mathbf{s}} = -\frac{(\bar{v}_1\,\Delta t - \bar{v}_{-1}\,\Delta t)}{(\mathbf{x}_1 - \mathbf{x}_{-1})}\hat{\mathbf{n}}, \tag{10}$$

or

$$\Delta\hat{\mathbf{s}} = -\frac{(\bar{v}_1 - \bar{v}_{-1})}{(\mathbf{x}_1 - \mathbf{x}_{-1})}\Delta t\hat{\mathbf{n}}. \tag{11}$$

Eqs (9) and (11) express the approximation to Huygens' principle used to track the wave propagation in the WS method.

In the limit of $|\mathbf{x}_1 - \mathbf{x}_{-1}| \to 0$ and $\Delta t \to 0$ (11) becomes

$$\frac{d\hat{\mathbf{s}}}{dt} = -(\nabla\bar{v}\cdot\hat{\mathbf{n}})\hat{\mathbf{n}}, \tag{12}$$

which states that the change in direction of the wave path is proportional to the gradient of the wavelength-averaged velocity in the direction normal to the wave path.

Equation (12) and the differential form of (9) for the change in wave location along the wave path,

$$\frac{d\mathbf{x}}{dt} = \bar{v}\hat{\mathbf{s}}, \tag{13}$$

are shown in Lomax (1992) to be equivalent to the differential equations for rays in geometrical ray theory with the local-medium velocity $c(\mathbf{x})$ replaced by the wavelength-averaged velocity $\bar{v}(\mathbf{x})$. In addition, putting $f \to \infty$ produces $\bar{v}(\mathbf{x}) \to c(\mathbf{x})$ (cf. eqs 1 and 2 with $T \to 0$), in which case expressions (12) and (13) become identical to the differential equations for ray theory. This property shows that in the limit of infinite frequency the WS method is the same as the geometrical ray method.

2.4 Free-surface reflections and conversions

The implementation of the WS method discussed in this work includes reflection and conversion of wave paths at the free surface but not at internal boundaries.

To include the effect of the free surface, the equations for plane-wave reflection and conversion (Savarensky 1975; Aki & Richards 1980) are evaluated whenever the wave location $\mathbf{x}_p$ reaches the surface $z = 0$. P to P, SV to SV and SH to SH surface reflections are performed with a simple reversal of the sign of the z component of the wave-path direction vector $\hat{\mathbf{s}}$. P to SV and SV to P conversions are applied by creating a new wave path, setting its direction using Snell's law and determining its amplitude using the plane-wave coefficients. The velocity values at instantaneous wavefront locations that lie above the free surface are determined from the velocity at the image locations obtained through reflection at the free surface.

Inhomogeneous P waves travelling along the surface can be created for SV to P conversions beyond the critical angle. Unfortunately, the numerical propagation of these inhomogeneous P waves in the present implementation of the WS algorithm is relatively time consuming because they travel along the surface and must be treated as continuous arrivals along the surface in contrast to the discrete arrivals of body waves.

When reflections and conversions at the free surface are included, the WS algorithm produces body waves and wave types that can be constructed with sums of body waves such as Love and inhomogeneous P waves. However, the WS method does not produce waves such as Rayleigh and Stoneley boundary waves, which do not have a duality with body waves.

2.5 Construction of synthetic seismograms

To generate synthetic seismograms, the wavelength-smoothing algorithm is used to trace many wave paths originating at different take-off angles from a point source. This set of wave paths is referred to as a *wave-path suite.* A different wave-path suite is generated for each of a range of centre frequencies f_n that cover the bandwidth of interest. After the wave-path suites for all frequencies have been calculated, wave arrivals at a given station are found by inspecting the surface arrivals of wave paths that were adjacent at the source to see if they bracket a region on the surface containing the station location. When such arrivals are found, an arrival time at the station is interpolated from the timing of the adjacent arrivals, and the amplitude is set in proportion to the geometrical spreading of the adjacent wave paths. The geometrical spreading is estimated from the ratio of the area of the surface between and normal to the wave paths of the adjacent arrivals to the area, defined by the same wave paths on the unit circle around the source. This spreading estimate is similar to methods used for estimating geometrical spreading in ray theory (Červený *et al.* 1977; Aki & Richards 1980) and is identical to an approximate method outlined in Červený *et al.* (1977, Section 3.5).

The response at a given station for each arrival at centre frequency f_n is formed by summing into a time series s_n. At the appropriate arrival time, a narrow-band filtered delta function δ_n is scaled to the arrival amplitude,

$$s_n(t, f_n) = \sum_j a_{jn}\delta_n(t - t_{jn}), \tag{14}$$

where a_{jn} is the amplitude and t_{jn} the arrival time of the jth arrival. The narrow-band delta function δ_n is formed by bandpass filtering a delta function between $f_n - \Delta f$ and $f_n + \Delta f$ where $\Delta f \sim (f_n - f_{n-1})$. The waveform examples presented in this work were constructed using non-causal filters, but causal filters may be more appropriate for some applications.

A broad-band time series $s(t)$ is constructed by summing together the narrow-band time series s_n from each modelled frequency,

$$s(t) = \sum_n s_n(t, f_n). \tag{15}$$

The time series $s(t)$ approximates the response at a given station to an impulsive source within the frequency band used for the wave-path suite calculations.

This band-limited, impulse response-time series can be convolved with a source–time function and a source-radiation pattern to produce a synthetic seismogram. The amplitude of the final synthetics is scaled to a particular scalar moment by insuring that the integral of the convolution of the band-limited, impulse response and the source–time function is equal to this moment.

The final time series will approximate the response to the P, SV or SH radiation from the source when the appropriate P or S model velocities are used for the wave-path calculations and the appropriate P, SV or SH radiation patterns are used for the construction of synthetics. However, since the implementation of the WS method discussed in this work does not include pre-critical reflections and wave-type conversions at internal discontinuities, the final time series will not be a complete representation of the wavefield.

In contrast to the velocity smoothing of the wave-path propagation algorithm, no form of wavelength-dependent spatial smoothing is employed in determining station arrival times and amplitudes. The lack of such a smoothing may lead to instability in the amplitude calculations and the shape of the final waveforms. Consequently, future development of the WS method may include spatial smoothing of the wave-path arrivals during construction of synthetic seismograms.

2.6 Application in a 3-D geometry

The implementation of the WS method in a 3-D geometry requires extension of the 2-D algorithms described above. Minor modifications include the specification in three-dimensions of the velocity model, the wave-path coordinates and station locations. More difficult is the modification of the algorithms for wavelength-averaged velocity and for the identification of arrivals and determination of geometrical spreading at a station.

For 3-D application, the wavelength-averaged velocity algorithm (eqs 4, 5 and 6) must be extended to smooth the velocity over a 2-D wavefront. This extension requires the determination of control point locations on the wavefront outwards from a central location and the use of 2-D forms of the weighting functions with maximums at the central location (Fig. 7).

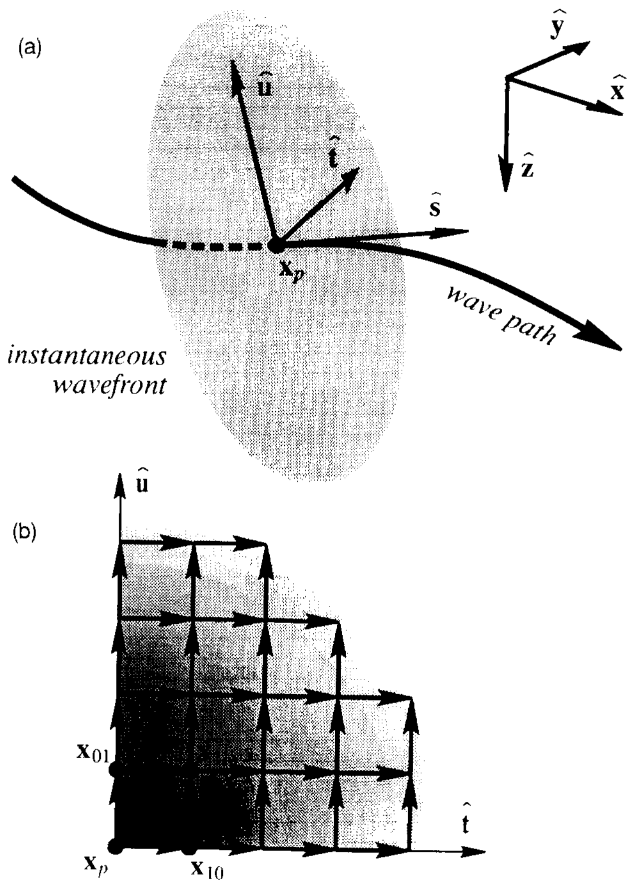

Figure 7. Wavelength-smoothing method in a 3-D geometry. (a) WS wave path, wavefront, global coordinates $\{x, y, z\}$, wave-path location $\mathbf{x}_p$ and wave-path centred coordinates $\{s, t, u\}$. (b) Calculation of control-point locations and relative weighting in one quadrant of the instantaneous wavefront. Control-point locations are estimated outwards from the wave-path location $\mathbf{x}_p$ as indicated by the arrows. Shading indicates the relative amplitude of the wavelength-dependent smoothing function across the instantaneous wavefront surface; darker shading indicates higher amplitudes.

3 BEHAVIOUR AND VALIDATION OF THE WAVELENGTH-SMOOTHING METHOD

In this section the WS method is compared with existing wave-propagation techniques, and it is shown to follow basic laws of ray and wave propagation. In addition, some of the critical parameters controlling the WS propagation algorithm are discussed and calibrated.

3.1 Wavelength-smoothing response to a simple crustal model

As an illustration of basic features of the WS method, consider *SH*-wave propagation from a point source in a reference homogeneous layer over half-space model. Fig. 8 shows this model geometry and the wave paths and reduced traveltimes for a WS simulation at four periods: 0.125, 0.5, 2.0 and 8.0 s. Note that the wavelengths in the upper layer at these periods are about $0.014h$, $0.07h$, $0.28h$ and $1.1h$ respectively, where h is the thickness of the layer. Free-surface reflections are not included in this example to allow characteristics of the direct wavefield to be examined.

At all four periods, the WS method produces direct and transmitted *S* wave paths and the wide-angle or post-critical reflection, *SmS* (Fig. 8). In the 2.0 s simulation a headwave phase, *Sn*, is defined by several arrivals between $90 < \Delta < 150$ km. A few *Sn* arrivals are also visible in the 0.5 and 0.125 s simulations; this phase would be better defined if the number of wave paths were increased.

The wave paths and traveltimes for the shortest period shown in Fig. 8, 0.125 s, are nearly identical to ray paths and traveltimes from standard ray-tracing methods. If even higher frequencies were used for the WS calculation, the corresponding wave paths and traveltimes would converge to those given by ray theory since the two methods are mathematically identical in the limit of infinite frequency (Lomax 1992). At longer periods, however, the WS wave paths and traveltimes differ from those of ray theory. This difference is indicated by comparing the 0.125 s WS results from those at 8.0 s in Fig. 8. At 8.0 s period, the *SmS* branch is reduced to a slight amplitude increase around $\Delta = 120$ km and all arrivals fall along a single, smooth traveltime branch, $\langle SmS{-}Sn \rangle$, near the *S* and *Sn* branches of ray theory.

3.1.1 *Behaviour of the wavelength-smoothing method at discontinuities*

At the discontinuity between the layer and the half-space in the model in Fig. 8, the WS method produces the transmitted *S*, the *Sn* and the *SmS* phases without any special treatment in the propagation algorithm of wave paths at this boundary. In contrast, these transmitted and reflected phases are not produced by the differential equations for ray paths which are not valid at velocity discontinuities. With the ray methods these phases are modelled by tracing incident rays to the boundary and applying conditions of continuity at the boundary to set the initial conditions for new rays introduced at the discontinuity (Červený *et al.* 1977).

Transmitted and reflected phases are produced directly in the WS method as a consequence of the smoothing of the medium velocity along the wavefront. The WS propagation algorithm actually produces only slowly varying refractions in this smoothed, 'virtual' medium, however, these refracted waves have the properties of sharply refracted (transmitted *S*), reflected (*SmS*) and diffracted (*Sn*) waves when considered in the context of the original medium.

It is noteworthy that the single WS algorithm models three wave phenomena, refractions, reflections and head waves, that must be treated separately with most other methods. This is an important aspect of the WS technique which allows the synthesis of significant features of the wavefield in models with complicated velocity variations. However, the WS method does not produce wave conversions in regions of large gradient in material properties which means that in such cases some wave types are ignored and that energy is not correctly partitioned along the wave paths.

In particular, the lack of a pre-critical reflection from the sharp discontinuity between the layer and the half-space is a characteristic of the WS method. This phase should appear between $\Delta = 0$ km and the distance of the frequency-dependent *Sn*–*SmS* cusp identified in Fig. 8. This phase is

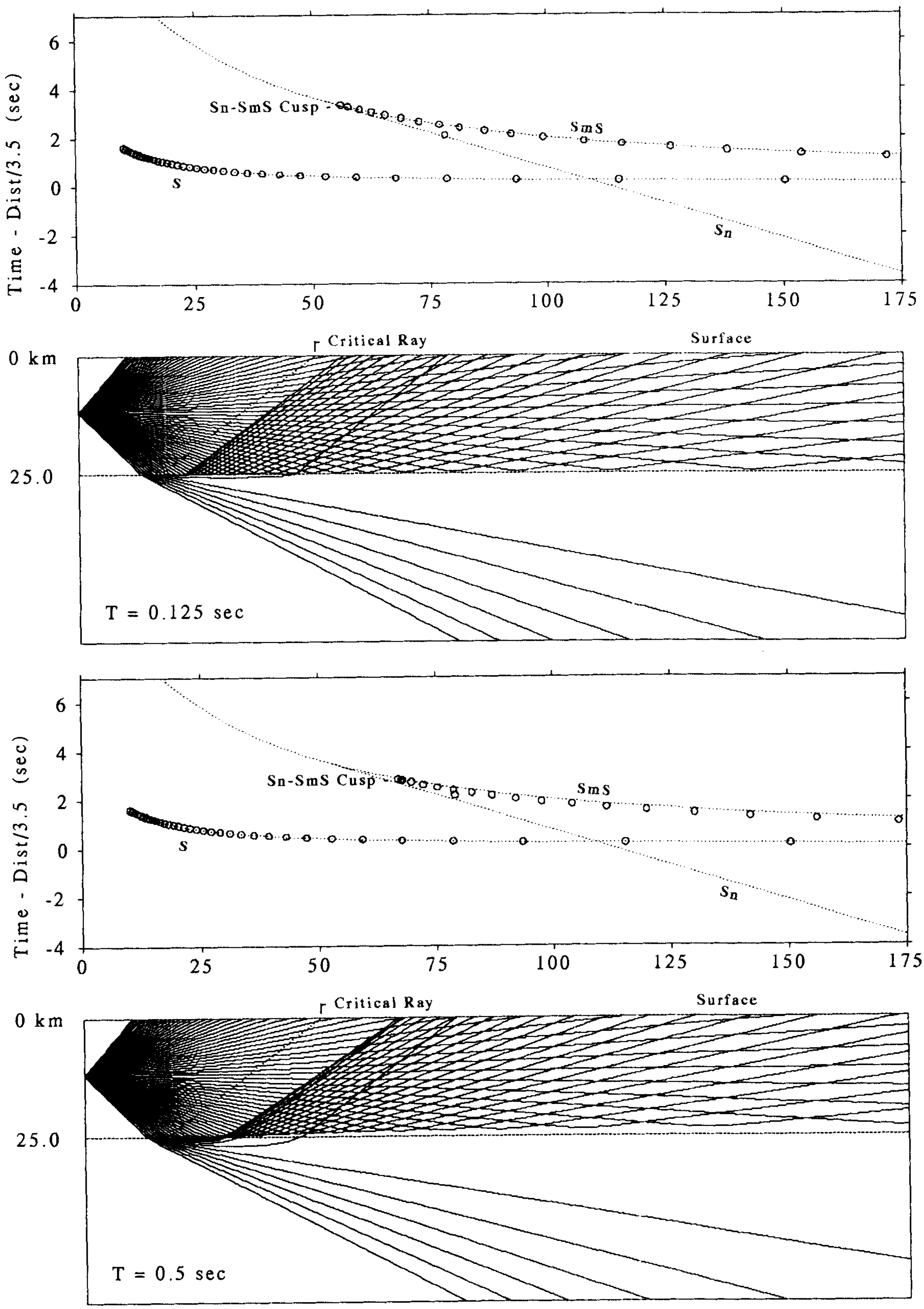

Figure 8. Wavelength-smoothing wave paths and traveltimes for S waves at 0.125, 0.5, 2.0 and 8.0 s period in a 25 km thick homogeneous layer over a homogeneous half-space velocity model. The layer and half-space have S-wave velocities of 3.5 and 4.4 km s^{-1} and densities of 2.6 and 3.3 gm cm^{-3}, respectively. The figures for each period: shows (bottom) the model and the wave paths in depth section, and (top) the traveltimes for all WS surface arrivals (circles). Traveltimes are plotted with a reduction velocity of 3.5 km s^{-1}. Each simulation shows 70 wave paths in a 95° fan originating at a point source at 12 km depth. The wavefront-movement calculation uses a Gaussian-weighting function with $\alpha = 2.0$ and $\theta_{max} = 1.5$. Approximate amplitudes for the waves are indicated by wave-path spreading and the density of arrivals on the traveltime plot. The critical ray of geometrical optics for this geometry is indicated by a dotted line on the depth section. Dotted lines on the traveltime plots show ray-theory traveltimes from a ray-tracing algorithm (Crossley 1986) for the S, SmS and Sn branches.

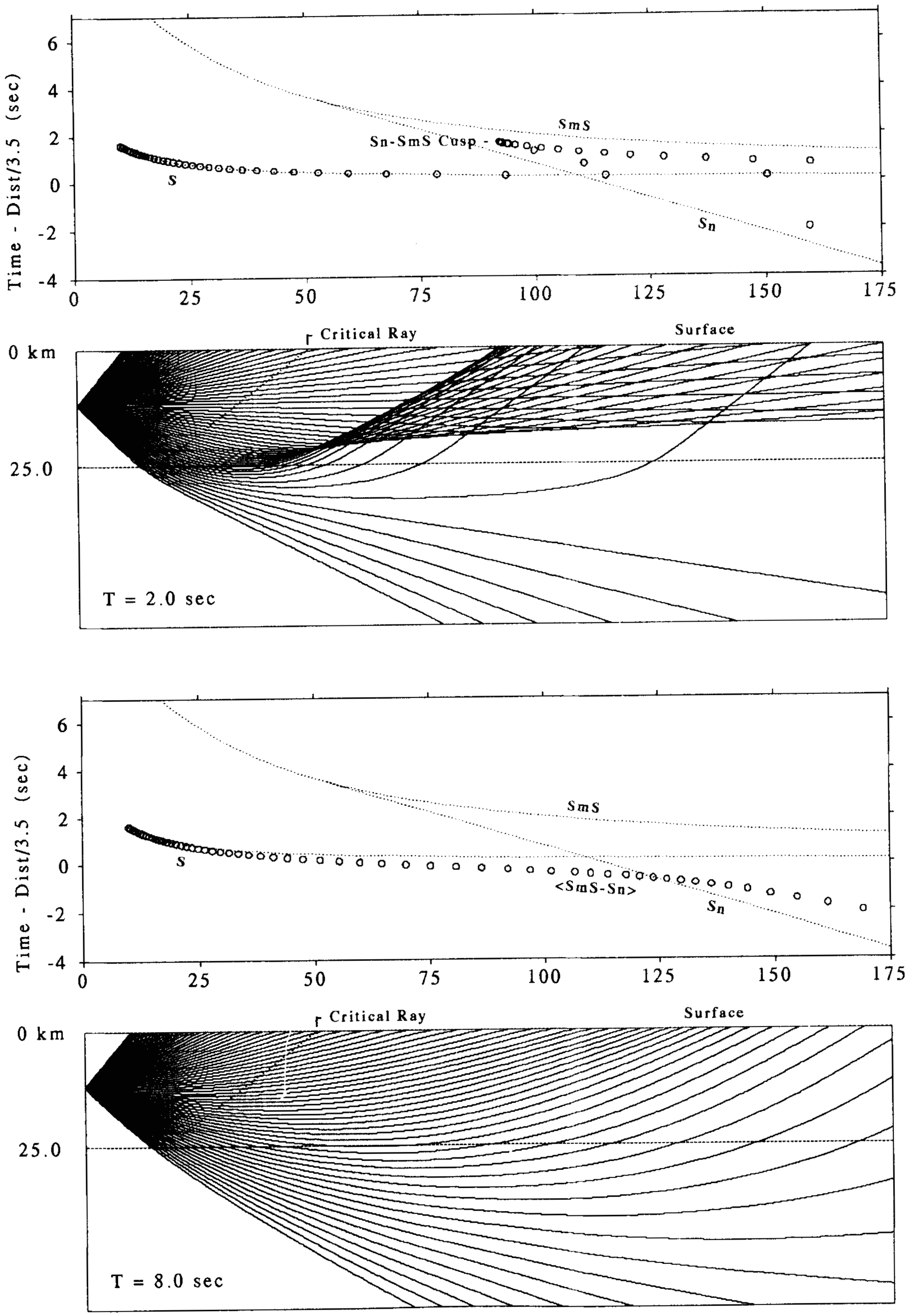

Figure 8. (*Continued.*)

not modelled because the velocity smoothing in the WS method transforms medium discontinuities into gradient zones.

The WS propagation algorithm only requires information about velocities at specific points in the model; it does not need information about the location, normal vectors, curvature or order of discontinuity of boundaries. A more complete treatment of wave propagation at sharp discontinuities requires the inclusion of logic in the WS algorithm for identification of interfaces as discontinuous surfaces and creation of new wave types at these interfaces in the manner of other techniques such as ray tracing (Červený *et al.* 1977) and in the Cagniard–DeHoop method (e.g. eqs 6.52 and 6.53 in Aki & Richards 1980). A preliminary investigation of modifications of the WS method indicates that wave propagation near a discontinuity must be modelled either by matching boundary conditions or by applying the WS propagation algorithm for all wave paths. It may be impossible to combine both techniques at a particular boundary because, at each frequency, the WS method responds to an effective, smoothed velocity distribution, while boundary-condition matching is always applied with respect to the original, unsmoothed discontinuity.

If boundary-condition matching were applied at selected discontinuities, the WS method would become structurally more similar to ray methods with the addition of frequency-dependent velocity smoothing in the regions between discontinuities. This extension to the WS method may improve its accuracy in situations where conversions or pre-critical reflections are significant.

3.1.2 *Frequency-dependent wave paths*

The results in Fig. 8 illustrate several important frequency-dependent effects of the WS method. At all but the longest periods, the direct *S* wave paths that pass entirely in the upper part of the layer have almost identical paths and traveltimes (compare the 0.125 and 2.0 s period simulations in Fig. 8). The traveltimes are similar because the instantaneous wavefronts for intermediate and shorter periods for the direct *S* phase lie almost entirely within the homogeneous layer and consequently produce nearly identical wavelength-averaged velocities and wave-path bending.

In contrast, reflected phases such as *SmS* that pass near the discontinuity at 25 km depth exhibit earlier arrival times and smoother wave paths as period increases (Fig. 8). These frequency-dependent wave paths lead to a simplification of the traveltime curves at longer periods as the *Sn–SmS* cusp shifts to greater epicentral distance. As will be shown later in an examination of synthetic seismograms, the change in *SmS* traveltimes with period imparts a frequency-dependent time delay that leads to a phase shift and dispersion in the reflected pulse in the final synthetics.

At an 8 s period the 25 km discontinuity reflection-branch *SmS* and the corresponding *Sn–SmS* cusps have nearly disappeared and the traveltime curve consists of two branches connected by a bend near $\Delta = 120$ km. Most of this traveltime curve before the bend ($40 < \Delta < 120$ km) has a slope corresponding approximately to the average velocity of the layer (3.5 km s^{-1}). The slope of the traveltime curve beyond the bend ($\Delta > 120$ km) corresponds to the velocity of the half-space (4.4 km s^{-1}). In contrast, arrivals at shorter periods in the region $\Delta > 50$ km occur along several distinct traveltime branches. At all periods, the first arrivals fall near the earliest traveltime curves predicted by ray theory.

All of the arrivals in the 8.0 s simulation for distances $\Delta > \sim 150$ km represent the *Sn*-headwave phase since the wave paths for these arrivals pass at or below the discontinuity through the top of the half-space. The greater number and corresponding increase in amplitude of the *Sn* arrivals at longer periods is in agreement with the theory that head waves have the form of the integral of the source-time pulse (Aki & Richards 1980) and consequently have more long-period content relative to direct waves and reflected waves.

The convergence of wave paths and clustering of arrivals on the shorter period traveltime plots at the cusp near the critical angle for *SmS* indicate that the WS method produces high amplitudes in these regions (Fig. 8). These high amplitudes are also produced with ray methods; they are a non-physical consequence of the caustic surface at the critical angle where the cross-section of the ray tube has vanishing area (Červený *et al.* 1977). Full-waveform methods would produce diffractions in this region. However, in contrast to geometrical ray theory, the location of the caustic surface and the cusp is frequency dependent in the WS method, moving to greater distance at longer periods (Fig. 8). This phenomena is predicted by theory for spherical waves impinging on a planar discontinuity and is referred to as *ray displacement* (Brekhovskikh 1980). In the WS method, the change in the position of the cusp allows a smoothing over frequency and space of the amplitude anomalies when a broad band of frequencies are summed to produce synthetic seismograms. This smoothing tends to damp the effect of the non-physical amplitude peaks and improves the stability of the WS method in critical regions.

The frequency-dependent wave paths are a direct consequence of the scaling of the velocity averaging with wavelength in the WS algorithm. The greater width of averaging along the instantaneous wavefront at longer periods causes the velocity contrast across the discontinuity to affect longer period wave paths at a greater distance than shorter period wave paths. This scaling effect can be seen by examining the bending and bottoming of the 0.125 and 2.0 s wave paths near the 25 km discontinuity in Fig. 8.

3.1.3 *Synthetic seismograms*

Figure 9 shows WS synthetic *SH* waveforms for the reference, homogeneous layer over half-space model from Fig. 8. The synthetics represent the along-strike response to a point strike-slip source and includes reflections at the free surface. The results for two source-time functions are shown, a broad-band, impulsive source with a period range of 0.18 to 32.0 s and a moderate bandwidth pulse with a centre period of 2.0 s.

Also included in Fig. 9 are synthetic waveforms for the same geometry and source functions produced by a normal-mode summation technique implemented by Robert Uhrhammer (private communication) following a method outlined in Aki & Richards (1980, Chapter 7). The normal-mode results give the numerical solution for the

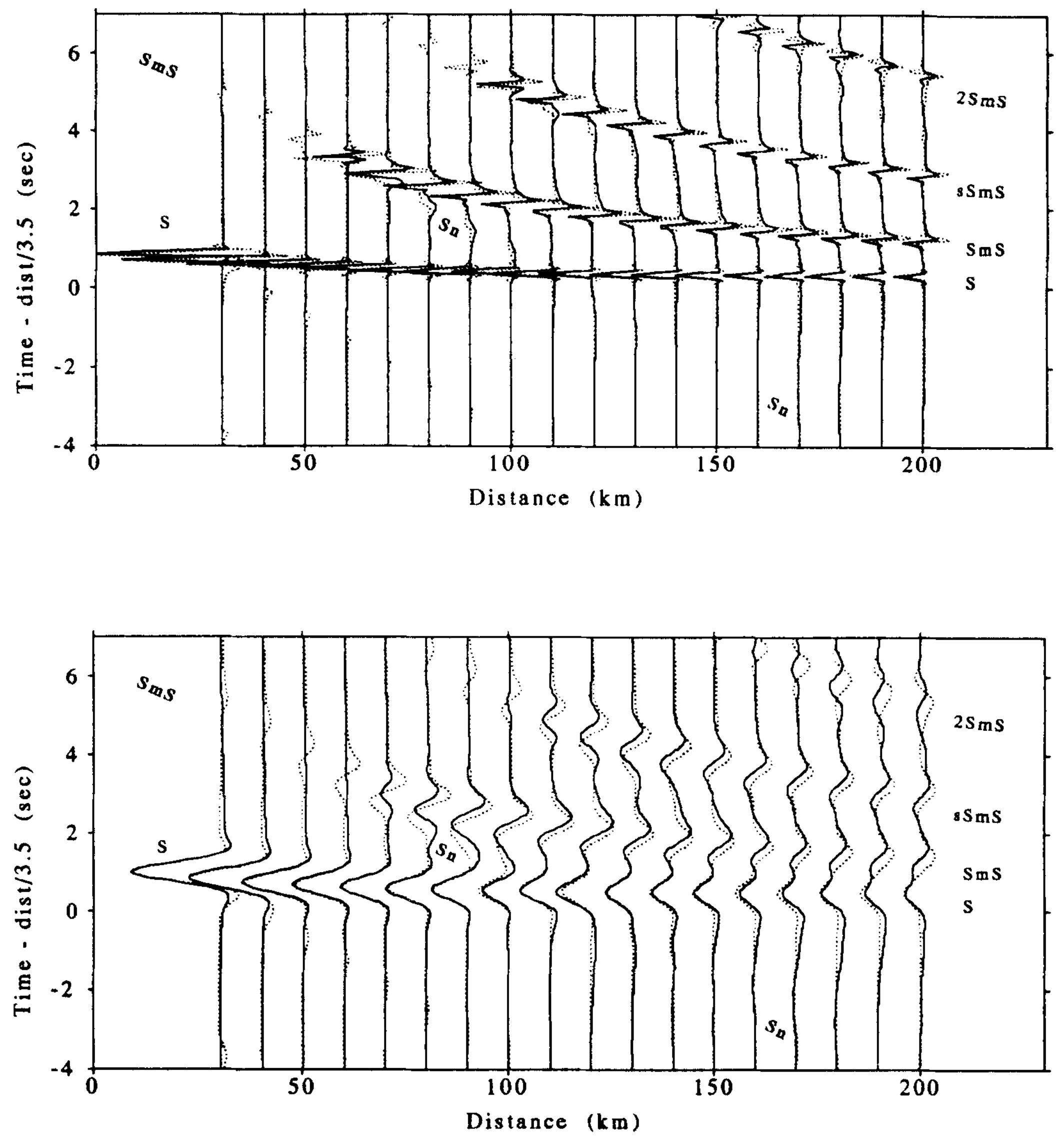

Figure 9. Wavelength-smoothing (solid) and normal-mode (dotted) *SH* synthetic seismograms for the homogeneous layer over the half-space velocity model and source location shown in Fig. 8. Synthetics are shown for two source types: (top) a broad-band impulse, and (bottom) a moderate bandwidth pulse. Reflections at the free surface are included. The small arrivals in the normal-mode synthetics before the direct *S* branch between 30 and 100 km are an artefact of frequency-domain processing and should be ignored. The WS weighting-function parameters are the same as those in Table 1.

complete, far-field response in this geometry and are taken as a standard measure for evaluation of the WS method.

The strongest arrivals produced in this simulation are the direct *SH* phase (*S*) and the wide-angle reflection at the 25 km discontinuity (*SmS*) and its multiple surface reflections (*sSmS*, *2SmS*). The headwave (*Sn*) and related reflected phases (*sSn*, *SmSSn*) form lower amplitude branches arriving earlier than, and tangent, to the corresponding reflected branches and converging with them at the critical distance.

Figure 9 indicates a fairly close match between the two methods for the direct *S* arrival and the post-critical reflections and surface multiples. In agreement with the normal-mode results, the direct *S* arrivals in the WS synthetics are nearly identical to the broad-band, impulse-source function. In contrast to the impulsive, direct *S* phase, the *SmS* arrival in both the normal-mode and the WS synthetics beyond 80 km has a distinct asymmetry. This asymmetry is related to a phase shift upon reflection at the discontinuity between the layer and the half-space. In the WS method, the asymmetry is produced by the phase advance of the longer periods relative to the shorter periods resulting from the reduced traveltimes of longer period waves that pass near the 25 km discontinuity. However, the phase shift in the WS method is significantly smaller than in the normal-mode results. This discrepancy may be related to the shape of the smoothing function and is discussed further below (Section 3.3.1).

The WS results match the character and timing of the normal-mode *Sn* phase where it is clearly visible ($80 < \Delta$ 100 km) on the impulsive-source synthetics in Fig. 9. However, there is some amplitude mismatch between the two methods, which may be related to the approximate modelling of the *Sn*-diffracted phase by a refraction in the WS method. The shape of the head waves in both methods is of the form of the integral of the source-time pulse. In the WS method this integration is produced by a delay in traveltime and an increase in amplitude of the longer period *Sn* arrivals relative to those at shorter periods; these effects are equivalent to the frequency-domain integration operation of dividing each spectral component by $i\omega$.

Significant shortcomings of the WS method apparent in Fig. 9 are the incorrect phasing of reflections near the critical distance and the lack of pre-critical reflections. These discrepancies can be seen in each reflection branch and are clearest on the impulsive-source synthetics.

3.2 The wavelength-smoothing method and basic laws of optics

In regions further than about a wavelength from discontinuities in the velocity structure, the wave propagation produced by the WS method follows the basic laws of optics concerning reflection and refraction at a plane discontinuity (Lomax 1992). This result is a direct consequence of the equivalence of the equations governing ray theory and those governing the wavefront movement in the WS method. However, close to a discontinuity, the WS wave paths at a given frequency do not locally follow the laws of optics on the original medium because the WS method is responding to a modified velocity distribution produced using the wavelength-averaged velocity.

3.3 Selection and calibration of wavelength-averaged velocity weighting functions

The WS method is characterized by the wavelength-dependent averaging of wave velocity across a surface normal to the wave path. Without this averaging the WS technique would not have any frequency dependence and would be identical to the geometrical ray method. Consequently, the justification, selection and calibration of the averaging algorithm are of crucial importance in the validation of the WS method as a new and useful tool.

3.3.1 Functional form of the weighting function

In this work a weighting function w with a Gaussian bell form is introduced (eq. 8); in Lomax (1992) two additional weighing functions, a cosine bell and the 'modified Fresnel' function are considered. All of these weighting functions have the form

$$w = w(\theta_n; N, \alpha, \theta_{max}), \qquad (16)$$

and the property

$$\lim_{|\theta| \to \infty} w = 0, \qquad (17)$$

where θ_n is distance along the instantaneous wavefront away from the wave path for the nth control point expressed in wavelengths, N is the total number of control points, θ_{max} is a truncation parameter and α is a width parameter.

The functional form of the weighting function and the width parameter α have a strong effect on the WS results. Because the spread of the smoothing function varies linearly with both the width parameter and period, a wave path for period T and width parameter $c\alpha$ will be identical to a wave path of period cT and width parameter α, where c is some constant. Consequently, the value of the width parameter α directly affects the assignment of wave-path arrivals to frequency in the construction of broad-band synthetics.

The reference, homogeneous layer over half-space model introduced above (Fig. 8) and the accurate normal-mode solutions for this model can be used to calibrate the parameters that define the velocity weighting function. As an illustration, consider the effect of varying the width parameter α. The preferred weighting function and time-step parameters are listed in Table 1. The WS results using these values along with normal-mode results were shown in Fig. 9.

In Figs 10 and 11 the effect of varying the weighting-function width parameter α is examined. When a smaller width is used ($\alpha = 1.0$; Fig. 10) there is no observable change in the direct *S* arrivals, but there is a significant deterioration in the phase match of later phases relative to the normal-mode results. In addition, the amplitude and sharpness of the *Sn* arrival is reduced relative to the $\alpha = 2.0$ WS results (Fig. 9). The poor match in the phasing of later arrivals is caused by a reduced difference in traveltime between waves of different frequencies when narrower smoothing functions are employed.

With a larger width parameter ($\alpha = 3.0$; Fig. 11) there is a slight improvement relative to the $\alpha = 2.0$ results of the match with the normal-mode synthetics of the phasing of reflected arrivals (*SmS*, *sSmS* and 2*SmS*). There are, however, changes in the direct *S* arrivals and the *Sn* arrivals resulting in a poorer match to the normal-mode results than that given by the $\alpha = 2.0$ synthetics. This change in *S* arrivals is clearest on the wide-band source synthetics where there is an amplitude instability on traces around 120 km and an underestimate of amplitudes at greater distances. For the *Sn* arrival, an increase in amplitude and a delay in the onset time relative to the $\alpha = 2.0$ WS results on the impulsive source synthetics gives a poorer match to the normal-mode results.

A similar comparison between the Gaussian, cosine and 'modified Fresnel' weighting functions using the layer over half-space model shows that the Gaussian weighting function is generally superior to the cosine and 'modified Fresnel' functions (Lomax 1992). However, the phase shift

Table 1. Preferred wavelength-smoothing propagation parameters

Parameter	Value
Weighting function	Gaussian
α (Width parameter)	2.0
θ_{max} (Truncation parameter)	1.5
N (Number of control points)	21 to 41
$T/\Delta t$ (Time-steps per period)	> 30

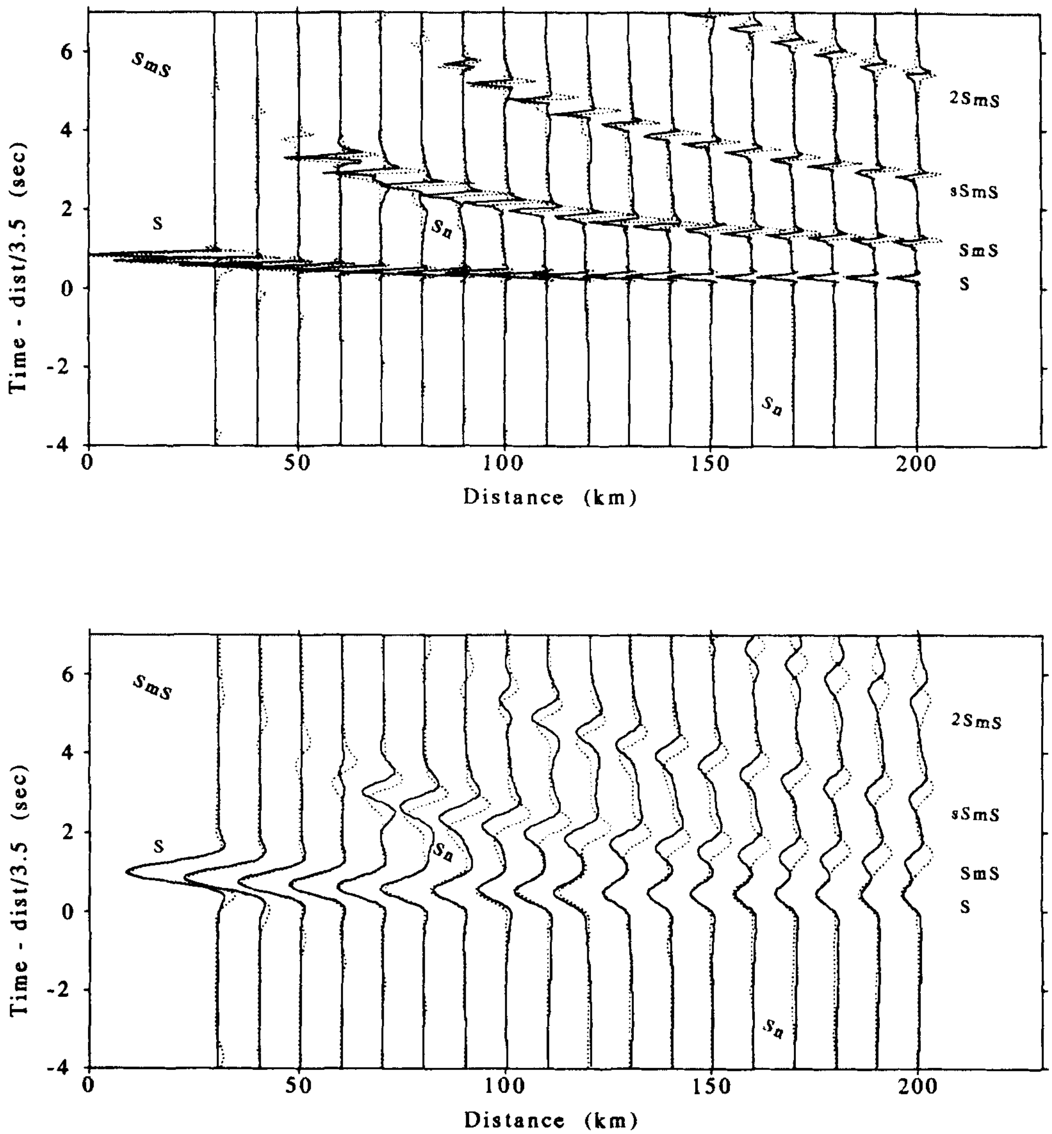

Figure 10. Synthetics using Gaussian-weighting function with $\alpha = 1.0$. Wavelength-smoothing (solid) and normal-mode (dotted) *SH* synthetic seismograms for the homogeneous layer over half-space model and source from Fig. 8 with the addition of reflections at the free surface. Synthetics are shown for two source types: (top) a broad-band impulse, and (bottom) moderate bandwidth pulse. The WS weighting-function parameters from Table 1 are used except for $\alpha = 1.0$.

of the reflected phases and the shape of the onset of the *Sn* phase in the 'modified Fresnel' synthetics match the normal-mode results better than the same features in the Gaussian weighting-function synthetics. Apparently the difference in shape of the 'modified Fresnel' weighting function relative to the Gaussian and cosine functions (Fig. 4) is significant; the 'modified Fresnel' weighting function and other weighting-function forms should be examined further in future work.

3.3.2 Selection of truncation parameter, time step and number of control points

The truncation parameter θ_{max} is relevant to the Gaussian and other weighting functions that asymptotically approach 0 as $\theta \rightarrow \infty$. The value of θ_{max} sets a cut-off distance along the instantaneous wavefront beyond which the weighting function is not applied. This parameter is not considered critical since the value of the wavelength-averaged velocity is expected to converge for large θ_{max}. Tests with the Gaussian weighting function indicate that a truncation of the tails at the point where the amplitude is around 1/100 of the maximum amplitude gives stable results. This is equivalent to a cut-off at about 1.5 times the half-width of the bell ($\theta_{max} = 1.5$). There is a trade-off between the truncation level and the spread of the control points. For a fixed number of control points, a larger truncation value θ_{max} increases the spread of the control points and can cause instabilities due to wide spacing of control points in high gradient portions of the velocity smoothing function.

In this work the number of control points, N, and the propagation time step, Δt, are each specified by two numbers giving the values at shortest and longest periods, respectively; the values of N and Δt for intermediate periods

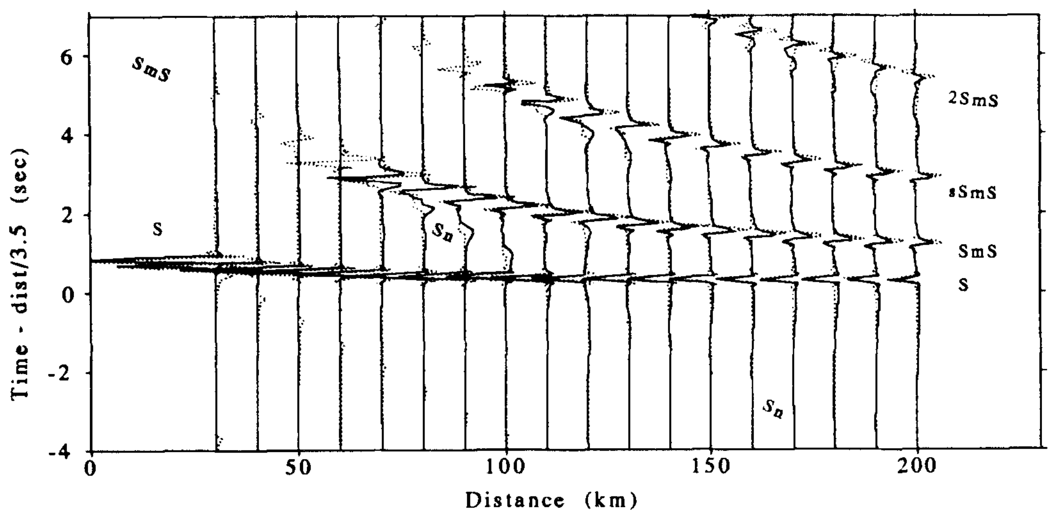

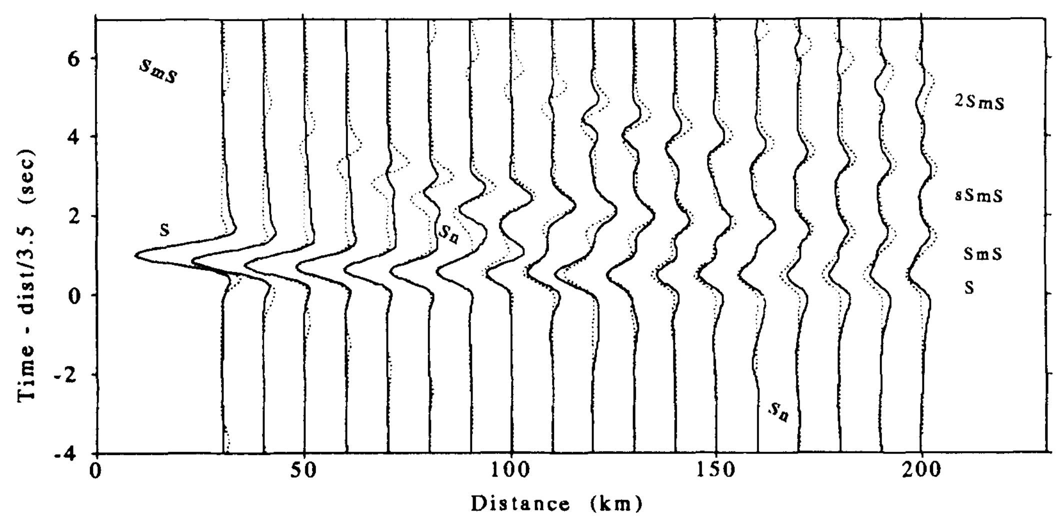

Figure 11. Synthetics using Gaussian weighting function with $\alpha = 3.0$. Wavelength-smoothing (solid) and normal-mode (dotted) *SH* synthetic seismograms for the homogeneous layer over half-space model and source from Fig. 8 with the addition of reflections at the free surface. Synthetics are shown for two source types: (top) a broad-band impulse, and (bottom) moderate bandwidth pulse. The WS weighting-function parameters from Table 1 are used except for $\alpha = 3.0$.

are set between the limiting values in proportion to the logarithm of period. The locations of WS wave paths and traveltimes along them will converge to limiting values as N becomes large and Δt becomes small. This convergence is illustrated in Fig. 12 which shows the effect of varying N and the ratio of period to time step, $T/\Delta t$, on the WS calculation for a single wave path. N and $T/\Delta t$ are comparable, period-independent measures that express the sampling of the medium in the WS algorithm perpendicular to and parallel to the wave path, respectively. The error in wave-path location as a percentage of total path length is shown for a wave path that has reflected off of the discontinuity in the reference layer over the half-space model (Fig. 8) for various values of N and $T/\Delta t$. The curves in Fig. 12 indicate that values of about 20 to 40 or greater for both N and for the ratio $T/\Delta t$ give a path error of about 1 per cent or less relative to the estimated converged path.

This error analysis is valid at all periods because it considers reflections from an infinite planar discontinuity which has no characteristic length. However, a similar analysis for a model with some characteristic length or lengths of velocity variation may indicate different, frequency-dependent optimum values for N and $T/\Delta t$. In particular, it may be important to vary the value of N as a function of period so that the spacing between weighting-function control points does not exceed the characteristic length of velocity variation in the model. For most models, a larger value of N should be used for longer periods. In a perfectly self-similar model, where the variation in velocity has no characteristic size, the value of N can be set independent of period.

In general, the values of N and Δt for a given period should be selected so that the distance between control points is similar to the distance the wave path moves in each

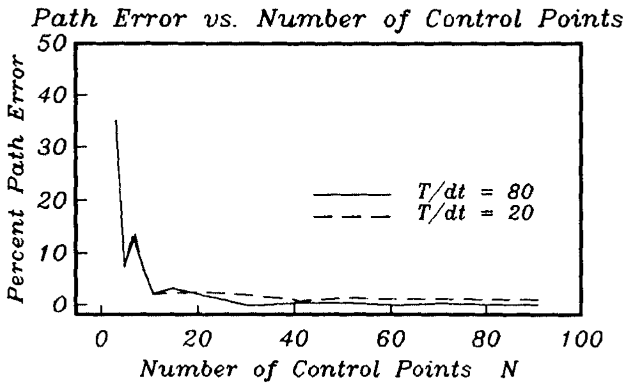

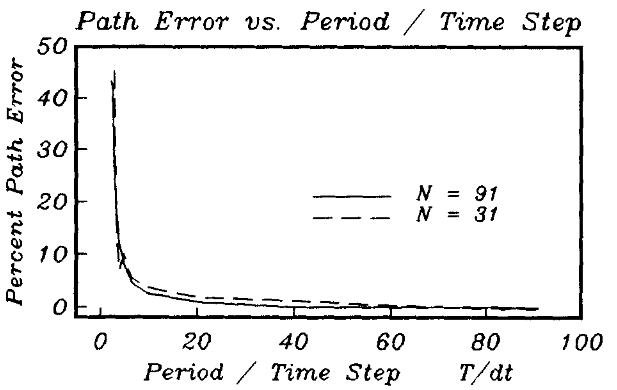

Figure 12. Wavelength-smoothing wave-path error as a function of: (top) number of control points N, and (bottom) number of time steps per period $T/\Delta t$ for a wave path that has reflected at a planar first-order discontinuity between homogeneous half-spaces. The path error is the ratio of the perpendicular distance between the wave path and the 'converged' wave path at a given location normalized by the path length between this location and the point of reflection. The 'converged' wave path is that given using the largest values of N and $T/\Delta t$. In each comparison error curves are shown for minimal acceptable values ($T/\Delta t = 20$, $N = 31$) and high values ($T/\Delta t = 80$, $N = 91$) of the fixed parameter N or $T/\Delta t$.

time step, that is,

$$\frac{\lambda_c}{N} \sim v_c \Delta t, \tag{18}$$

where λ_c is a characteristic wavelength for the model and v_c is a characteristic velocity. This relation ensures that the model is sampled at a similar spacing parallel and perpendicular to the wave path. Since $\lambda_c = v_c T$ where T is the period, expression (18) reduces to

$$N \sim \frac{T}{\Delta t}. \tag{19}$$

This result is compatible with the values for N and $T/\Delta t$ found above in the wave-path error analysis.

4 THE WAVELENGTH-SMOOTHING METHOD IN COMPLEX STRUCTURES

The preceding investigations of the WS method are for simple, highly symmetric models. It is important to examine the accuracy of the WS method in complex models which cannot be modelled efficiently by existing methods.

4.1 Rough-interface model

In this section, comparisons are presented between the WS method and a boundary-integral technique (Bouchon & Aki 1977) for wave propagation in a laterally varying medium. A boundary-integral method implemented by Olivier Coutant (private communication) using a discrete wavenumber description of Green's functions (Campillo & Bouchon 1985) is used in the following comparisons. This discrete wavenumber–boundary-integral method (DW–BI) produces the complete incident, reflected and diffracted field over a limited frequency band for *SH*-wave propagation in a 2-D model consisting of two homogeneous regions separated by a rough interface.

For the following comparisons, WS synthetics for a broad-band, impulsive source are produced using the preferred weighting-function parameters from Table 1. Because it is a 2-D formulation, the DW–BI method produces the response to a line source; this response includes a $1/\sqrt{t}$ decay in the pulse shapes. To produce equivalent, line-source seismograms, the WS synthetics include 2-D geometrical spreading and are convolved with the DW–BI synthetic for a homogeneous whole-space.

Relative to the DW–BI calculations, the WS calculations are an order of magnitude faster, require a small fraction of the computer memory and cover a broader band of frequencies.

4.1.1 Plane interface

To illustrate the DW–BI method and the accuracy of the WS technique, both methods are first applied to the homogeneous layer over the half-space model discussed earlier (Fig. 8). Synthetic seismograms for the response at the surface are shown in Fig. 13. The DW–BI synthetics include the direct *S* phase, the reflection from the base of the layer (*SmS*) and the head wave (*Sn*). The WS synthetics match the direct *S*, the wide-angle *SmS* reflection (distance $\Delta > \sim 100$ km) and the *Sn* phases closely, but do not produce the pre-critical *SmS* reflection ($\Delta < \sim 90$ km). The WS amplitudes are larger than the DW–BI amplitudes in the region $110 < \Delta < 130$ km; this amplitude increase can be attributed to non-physical, high-amplitude arrivals in the WS method at the frequency-dependent critical distance. In the region $\Delta > 130$ km the WS amplitudes for the combined direct *S* and *SmS* pulse are smaller and there is some distortion of the earlier *Sn* waveform relative to the DW–BI results. These differences may be related to the approximate modelling in the WS method of a diffracted phase, *Sn*, with a refraction algorithm. In the WS simulation, the energy that should form the pre-critical reflection at $\Delta < \sim 90$ km and diffractions at $\Delta > 130$ km is mapped into the region $110 < \Delta < 130$ km.

4.1.2 Rough interface

Figure 14 shows a rough interface model and WS wave paths and traveltimes at high frequency and at an intermediate period for an *SH*-line source in the layer above the interface. The amplitude of the interface is described by a

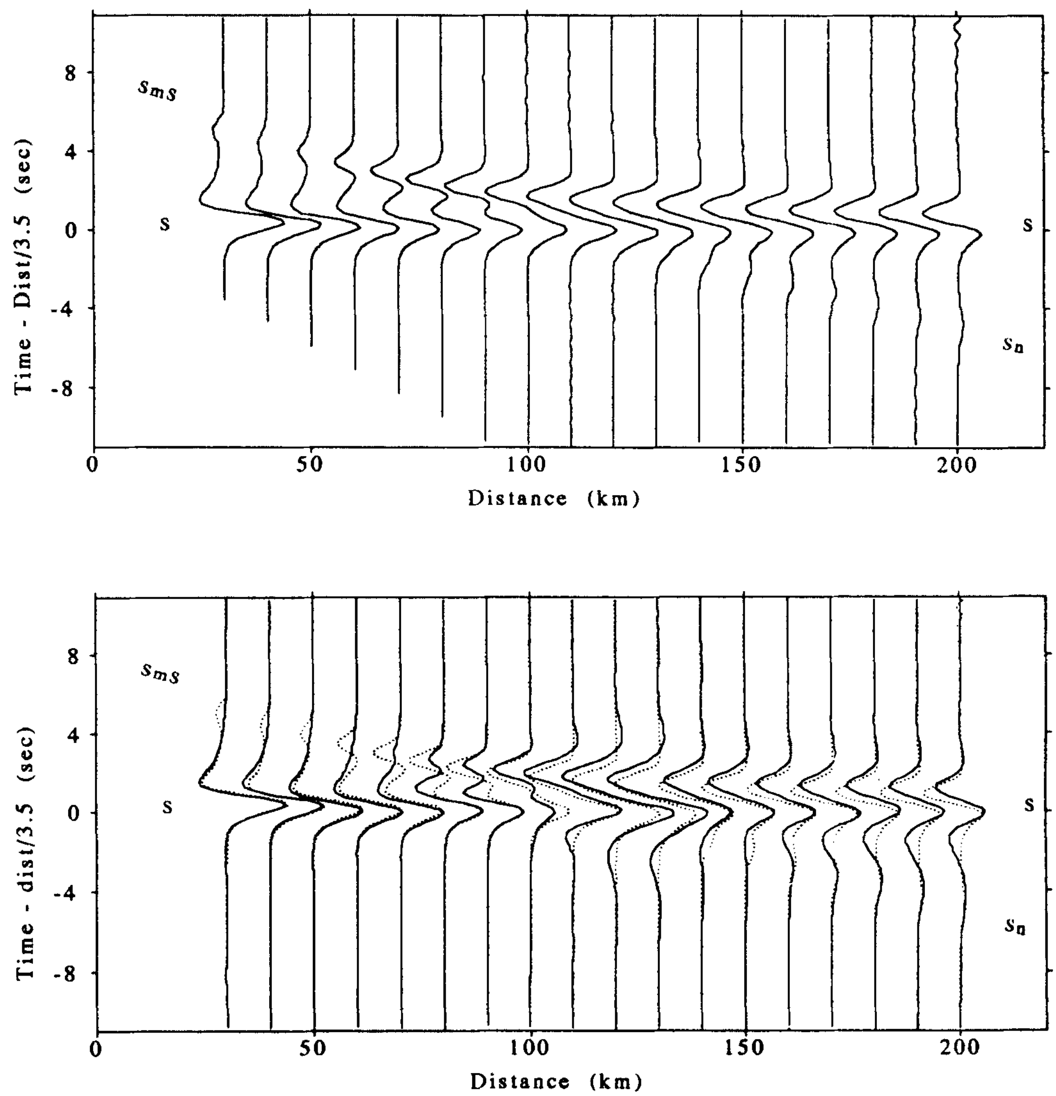

Figure 13. Synthetic seismograms for the flat-boundary velocity model of Fig. 8. Upper: discrete-wavenumber–boundary-integral (DW–BI) synthetics. Lower: wavelength-smoothing synthetics (solid) and DW–BI synthetics (dotted). All synthetics represent the response to a low-pass filtered, doubly integrated, step-function source.

sum of sinusoids centred at a mean depth z_0,

$$z(x) = z_0 + \sum_k A_k \sin(2\pi x/\lambda_k), \tag{20}$$

where x is horizontal distance, z is depth, A_k is the amplitude and λ_k the wavelength of the kth sinusoid. The model described in Fig. 14 is a simplified 2-D characterization of complicated vertical and lateral crustal-velocity variations that may exist in many parts of the world. In the current analysis, this structure is of interest as an illustration of the validity and accuracy of the WS method in realistic complex structures.

The wave paths in Fig. 14 show the effect of frequency-dependent smoothing in the WS method in complex models. Short-period wave paths with wavelengths much smaller than the scale of undulations of the rough boundary ($T = 0.25$ s) are scattered by this boundary producing a chaotic traveltime signature. The longer period wave paths ($T = 2.8$ s) are affected more coherently by the boundary, producing a region of focusing at $110 < \Delta < 150$ km.

Figure 15 shows the DW–BI and WS synthetics for the rough boundary model of Fig. 14. The DW–BI rough-boundary synthetics are significantly different from the DW–BI flat-layer synthetics (Fig. 13) for all phases except the direct S at $\Delta < 90$ km. Notable differences include the lack of a coherent pre-critical SmS reflection at $\Delta < 90$ km, the deterioration of the SmS reflection and corresponding change in waveforms at $90 < \Delta < \sim 150$ km and the reduced amplitude of the combined direct S and SmS phase at $\Delta > \sim 150$ km. There is also a striking change in the waveforms between $\Delta = 150$ and $\Delta = 160$ km due to a partial shadow zone beyond 150 km.

The WS synthetics for the rough boundary model (Fig. 15) match the main features on the DW–BI synthetics at all distances except for $\Delta = 150$ km. The lack of coherent pre-critical reflections in the DW–BI synthetics is matched by the WS results simply because this phase is neglected in the WS algorithm. Also, the excellent match of the WS direct S phase at $\Delta < 90$ km to the DW–BI waveforms is of minor interest since this phase is little affected by the rough boundary. However, the reproduction by the WS method of significant features of the DW–BI waveforms at $\Delta > 90$ km indicates that the approximate WS algorithm responds well to the complex, rough-boundary model. In particular, the WS synthetics correctly predict the overall change in shape and amplitude between waveforms at $\Delta < 150$ km and those at $\Delta > 150$ km.

There is a significant mismatch in amplitude between the WS and DW–BI synthetics at $\Delta = 150$ km. Here, an increased amplitude in the WS waveform is caused by the focusing and convergence of wave paths reaching the surface near $\Delta = 150$ km (Fig. 14). The simple technique used in the WS algorithm for estimating amplitudes based on the spreading of adjacent wave paths is unstable in regions where wave paths converge. While non-physical, high amplitudes are to be expected in such regions in both the WS and basic ray methods, it is likely that the WS method can be modified to reduce the significance of amplitude singularities. Such modifications might include the use of amplitude-estimation techniques from advanced ray methods (Červený *et al.* 1977) or the use of a wavelength-dependent spatial smoothing of amplitude in the construction of WS synthetics.

There is also some difference in the shape of the WS waveforms relative to the DW–BI waveforms beyond $\Delta = 150$ km that may be related to the amplitude anomaly at $\Delta = 150$ km. Some of the energy arriving beyond this distance in the more accurate DW–BI simulation probably is caused by diffractions from the high-amplitude wavefield arriving near $\Delta = 150$ km. In the WS method, the energy that would contribute to this diffraction is contained in the focused wave paths arriving near $\Delta = 150$ km (Fig. 14) and contributes to the high-amplitude singularity. There is the possibility that an improved treatment of the amplitude instability at $\Delta = 150$ km may lead to an improvement in the waveforms shapes for $\Delta > 150$ km.

Overall, the WS method reproduces approximately most of the features of the accurate DW–BI synthetics from both the flat layer and rough-interface models. And, the WS computations for both models are an order of magnitude faster than the DW–BI computations. These are important results because they indicate that the approximate WS

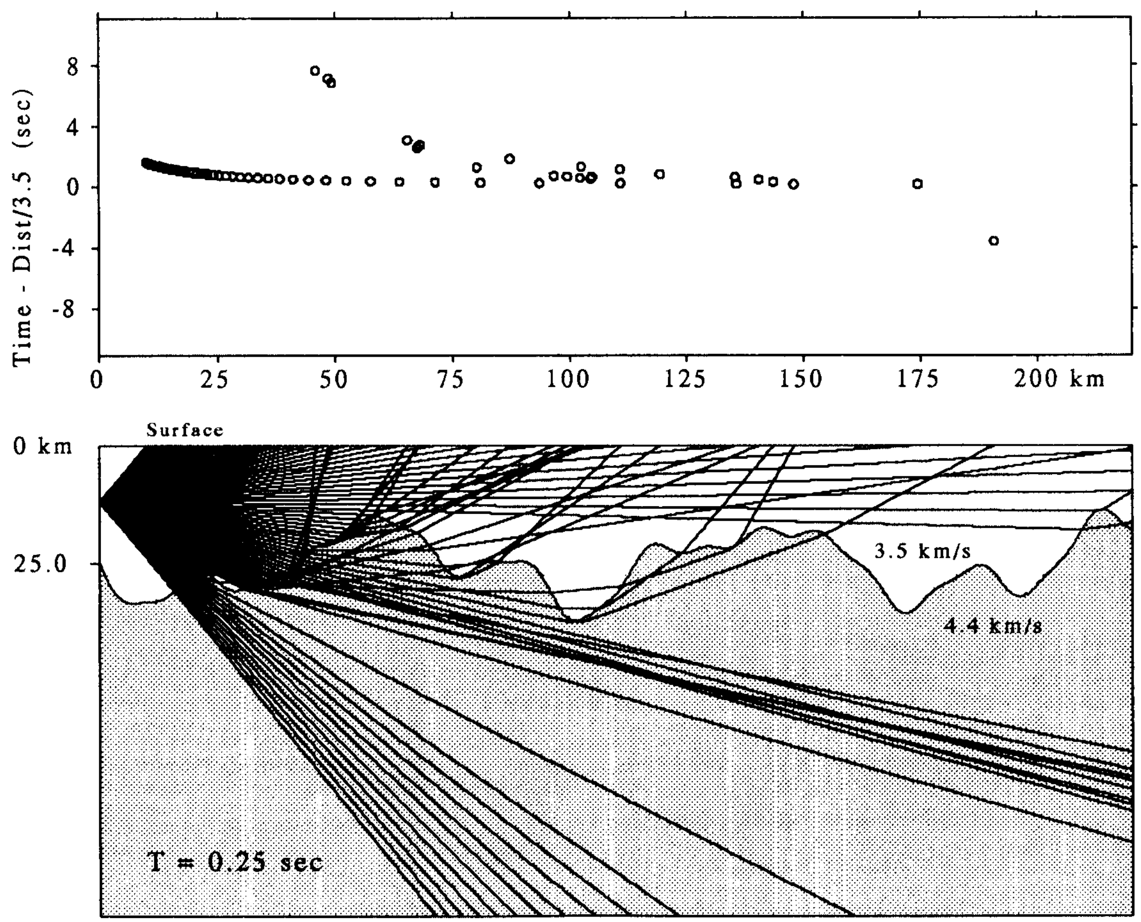

Figure 14. Rough-boundary velocity model and wavelength-smoothing results for periods of 0.25 and 2.8 s. The model consists of a homogeneous layer over a homogeneous half-space separated by an irregular boundary. The model parameters are otherwise the same as in Fig. 8. The boundary parameters from eq. (20) are $z_0 = 25$ km; $k = 1,4$; $A_k = \{2, 4, 7, 14\text{ km}\}$; $\lambda_k = \{12, 24, 32, 80\text{ km}\}$. The figure for each period shows: (lower) a cross-section of the model and WS wave paths, and (upper) the reduced traveltimes for surface arrivals plotted as a function of epicentral distance.

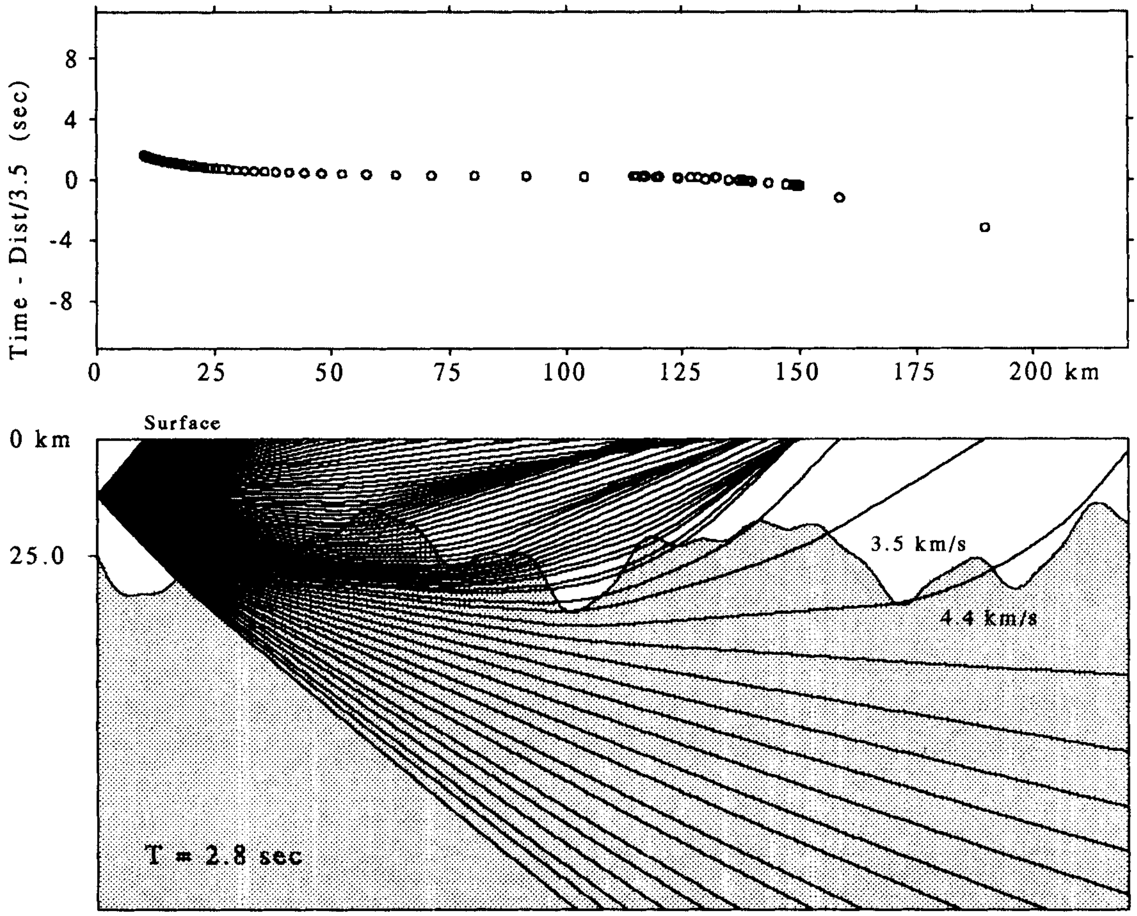

Figure 14. (*Continued.*)

method may be a useful tool for modelling wave propagation in complex models, although further numerical testing and theoretical development of the method is required.

DISCUSSION

The WS method is intended for the modelling of broad-band seismic-wave propagation in geologic structures with complicated wave-velocity variations. This approximate, numerical method has been developed based on the premise that waves at a given period respond to all variations in material properties as if these properties were smoothed over space in proportion to the local wavelength. Wave paths are moved through space using an approximation to Huygens' principle applied using the wavelength-smoothed velocity values.

Analysis with the WS method is analogous to the repeated application of geometrical ray tracing through different, smoothed versions of a particular velocity model. However, unlike the somewhat arbitrary model smoothing that is often applied before the use of ray and other methods, the smoothing in the WS method is given an explicit frequency dependence. Also, the smoothing is performed dynamically as a function of the position and orientation of the instantaneous wavefronts. The WS technique therefore avoids the significant computational overhead that would be required to calculate and store smoothed versions of an initial model.

It should be noted that the WS method, with its wavelength smoothing, appears similar to extensions to the ray method such as the Gaussian-beam method (Červený, Popov & Pšenčík 1982; Červený 1983) and Fresnel-volume ray tracing (Červený & Soares 1992), both of which involve finite beam widths. However, there are significant differences between these techniques and the WS method which underscore the uniqueness of the WS method (Appendix A).

The wavelength-smoothing method produces the following wave types and wave phenomena over a broad frequency range.

(1) Refracted direct waves are accurately reproduced in homogeneous or smoothly varying regions.

(2) Transmitted refractions, wide-angle reflections and head waves are reproduced approximately at discontinuities.

(3) Frequency-dependent scattering of some wave types is reproduced as a function of the ratio of wavelength to characteristic size of scattering region.

(4) A portion of the diffracted energy is produced in geometrical shadow regions.

However, the wavelength-smoothing method as currently

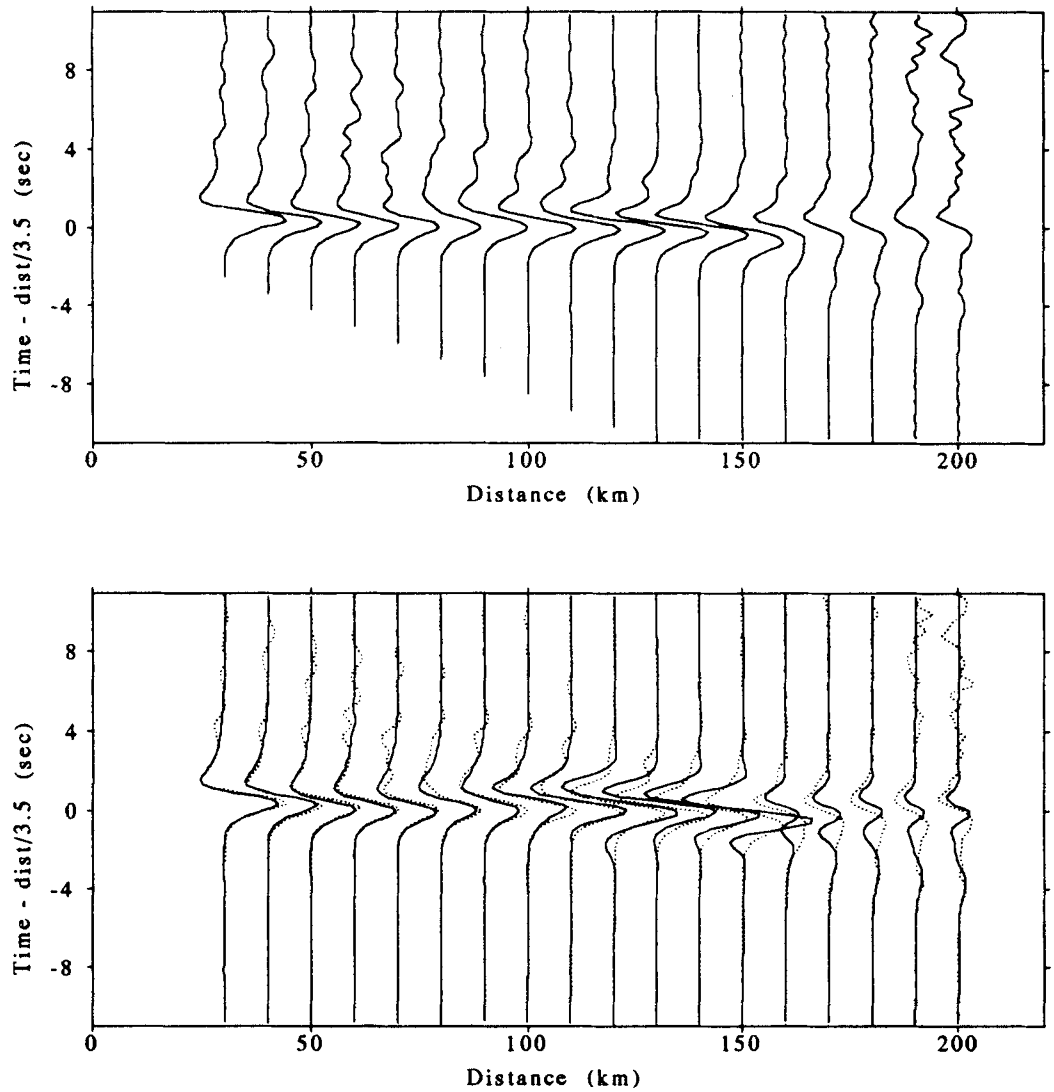

Figure 15. Synthetic seismograms for the rough-boundary velocity model of Fig. 14. Upper: discrete-wavenumber–boundary integral (DW–BI) synthetics. Lower: wavelength-smoothing synthetics (solid) and DW–BI synthetics (dotted). All synthetics are convolved with the same low-pass filtered, doubly integrated step-function source. The late, low-amplitude signal on the DW–BI synthetics at $\Delta \leq 100$ km is due to scattered, pre-critical reflections from the rough boundary. The high-frequency oscillation at $\Delta \geq 150$ km and the higher amplitude noise for $t > \sim 1$ s at $\Delta \geq 180$ km on the DW–BI synthetics are a consequence of computational limitations and should be ignored.

formulated does not reproduce some features of the complete wavefield and has certain instabilities. These deficiencies include the following points.

(1) In regions with strong velocity gradients there are no pre-critical reflections or wave-type conversions.

(2) In critical regions where the geometrical spreading function is small or singular there may be instability in the amplitude estimates.

(3) There is incomplete modelling of diffracted waves in geometrical shadow regions.

(4) The use of a finite number of wave paths can lead to poor sampling of parts of the structure and inaccurate synthesis of corresponding parts of the wavefield.

(5) The wavelength-smoothing method is a kinematic technique which approximates scalar-wave propagation; this method does not produce many elastic-wave phenomena.

The features and shortcomings of the wavelength-smoothing algorithm are a consequence of its tracking refractions only in a smoothed version of the original velocity model. In particular, the first three shortcomings are related because the WS method maps some of the wave energy that should form pre-critical reflections, converted wave types and diffractions into refractions in singular regions. This shifting of energy leads to the amplitude instability in waveforms near-critical regions.

Most of the shortcomings discussed above are also found in geometrical ray tracing; however, some are less serious in the WS method as a consequence of its frequency dependence. Many of the deficiencies of the WS method may be minimized as the method is further developed, perhaps using techniques from extensions to the ray method.

The WS method, though not strictly derived from basic equations, produces many expected broad-band wave phenomena in simple and complicated velocity structures. However, future work on the method should include investigation of a formal derivation of the propagation algorithm, perhaps making further use of the Helmholtz–Kirchhoff integral theorem, by examination of Fresnel zones (e.g. Červený & Soares 1992) or using concepts of 'wave paths' in diffraction tomography (Woodward 1992).

In addition to the modifications to the WS method discussed above with regards to shortcomings of the method, other extensions to the algorithm may be of use in many seismological studies. For example, the WS method can be easily modified to include intrinsic attenuation through the specification of the quality factor Q (Bullen & Bolt 1985) in the velocity model and the WS method can be used in inversion for velocity structure since the wave paths between source and receiver are known.

ACKNOWLEDGMENTS

This paper is a summary of part of my PhD work at the University of California at Berkeley. I am grateful to my advisor Professor Bruce Bolt for his consistent support for my research on the WS method. I thank Olivier Coutant, Valeri Korneev and Robert Uhrhammer for their assistance in the implementation of established methods for modelling seismic-wave propagation and I thank Barbara Romanowicz, Douglas Dreger, Bruce Bolt and two anonymous reviews for their extensive and helpful comments.

REFERENCES

Aki, K. & Richards, P.G., 1980. *Quantitative Seismology: Theory and Methods,* W.H. Freeman, San Francisco.

Bolt, B.A. & Dorman, J., 1960. Phase and group velocity of Rayleigh waves in a spherical, gravitating earth, *J. geophys. Res.,* **66,** 2965–2981.

Bouchon, M. & Aki, K., 1977. Discrete wavenumber representation of seismic source wave fields, *Bull. seism. Soc. Am.,* **67,** 259–277.

Brekhovskikh, L.M., 1980. *Waves in Layered Media,* Academic Press, New York.

Bullen, K.E. & Bolt, B.A., 1985 *An introduction to the theory of seismology,* Cambridge University Press, Cambridge.

Campillo, M. & Bouchon, M., 1985. Synthetic *SH* seismograms in a laterally varying medium by the discrete wavenumber method, *Geophys. J.R. astr. Soc.,* **83,** 307–317.

Červený, V., 1983. Synthetic body wave seismograms for laterally varying layered structures by the Gaussian beam method, *Geophys. J. R. astr. Soc.,* **73,** 389–426.

Červený, V., 1985a. Ray synthetic seismograms for complex two-dimensional and three-dimensional structures, *J. Geophys.,* **58,** 2–26.

Červený, V., 1985b. Gaussian beam synthetic seismograms, *J. Geophys.,* **58,** 2–26.

Červený, V. & Soares, J.E.P., 1992. Fresnel volume ray tracing, *Geophysics,* **57,** 902–905.

Červený, V., Molotkov, I.A. & Pšenčík, I., 1977. *Ray Method in Seismology,* Univerzita Karlova, Prague.

Červený, V., Popov, M.M. & Pšenčík, I., 1982. Computation of wave fields in inhomogeneous media–Gaussian beam approach, *Geophys. J. R. astr. Soc.,* **70,** 109–128.

Crossley, D., 1988. *RAYAMP–PC for IBM–PC and compatible microcomputers,* Geophysics Laboratory, McGill University, Montreal.

Dziewonski, A.M. & Anderson, D.L., 1981. Preliminary reference Earth model, *Phys. Earth planet. Inter.,* **25,** 297–356.

Elmore, W.C. & Heald, M.A., 1985. *Physics of Waves,* Dover, New York.

Frankel, A., 1989. A review of numerical experiments on seismic wave scattering, *Pure appl. Geophys.,* **131,** 639–685.

Frankel, A. & Vidale, J., 1992. A three-dimensional simulation of seismic waves in the Santa Clara Valley, California, from a Loma Prieta Aftershock, *Bull. seism. Soc. Am.,* **82,** 2045–2074.

Fuchs, K., 1968. The reflection of spherical waves from transition zones with arbitrary depth-dependent elastic moduli and density, *J. Phys. Earth,* **16,** 27–41.

Hong, T.-L. & Helmberger, D.V., 1978. Glorified optics and wave propagation in non-planar structures, *Bull. seism. Soc. Am.,* **68,** 1313–1330.

Igel, H., Mora, P., Rodrigues, D., Leary, P. & Ben-Zion, Y., 1991. Finite difference simulation of fault zone trapped waves on the massively parallel connection machine, Abstract, *EOS, Trans. am. geophys. Un.,* **72,** (44), 307.

Lomax, A.J., 1992. An approximate method for modelling broadband wave propagation through complex, inhomogeneous media, *PhD thesis,* University of California at Berkeley.

Lomax, A. & Bolt, B.A., 1992. Broadband waveform modelling of anomalous strong ground motion in the 1989 Loma Prieta earthquake using three-dimensional geologic structures, *Geophys. Res. Lett.,* **19,** 1963–1966.

Officer, C.B., 1958. *Introduction to the Theory of Sound Transmission,* McGraw-Hill, New York.

Richards, P.G., Witte, D.C. & Ekstrom, G., 1991. Generalized ray theory for seismic waves in structures with planar nonparallel interfaces, *Bull. seism. Soc. Am.,* **81,** 1309–1331.

Savarensky, E., 1975. *Seismic Waves,* (English translation), Mir Publishers, Moscow.

Spudlich, P. & Archuleta, R.J., 1987. Techniques for Earthquake Ground-Motion Calculation with Applications to Source Parameterization to Finite Faults, in *Seismic Strong Motion Synthetics,* pp. 205–265, ed. Bolt, B.A., Academic Press, Orlando.

Woodward, M.J., 1992. Wave-equation tomography, *Geophysics,* **57,** 15–26.

APPENDIX A

The WS technique is often compared with the Gaussian-beam method since both involve exponential bell functions and a nominal, finite wave-path width. Consequently, it is important to note some fundamental aspects of the Gaussian-beam method that help to distinguish the WS method from it. First, the finite width of the Gaussian beam contributes *amplitude* and *phase* information only to the solution and does not influence the beam *paths.* The paths are traced using standard ray theory before application of the beam methodology. In the WS method the wave paths are frequency dependent. Second, in constructing the Gaussian-beam solution the elastic properties away from the central ray are estimated with a Taylor expansion using the elastic properties and their derivatives evaluated only at the central ray. Consequently, the Gaussian-beam method is restricted to smoothly varying media and the solutions are exact only for a *virtual medium* defined by the properties at the central ray. When the beam width becomes large the virtual medium properties may differ significantly from the actual medium. In particular, the solutions may be inaccurate near strong lateral variations (Červený 1985b). In contrast, the velocity smoothing in the WS method makes explicit use of medium properties at finite distances from the wave paths. Finally, the Gaussian-beam method is defined as a *high-frequency* method only, while the WS method is developed for *broad-band* modelling.

Another aspect of the Gaussian-beam method to note is that the initial beam width is not determined *a priori.* In practice the optimum beam-width parameter depends on the geometry of the model (Červený 1985b). In the WS method there is a similar, smoothing-width factor (e.g. α in eq. 3) which, in the present propagation algorithm, is also not determined theoretically.